Oceanic Cyclogenesis as Induced by a Mesoscale Convective System Moving Offshore. Part I: A 90-h Real-Data Simulation

DA-LIN ZHANG AND NING BAO

Department of Atmospheric and Oceanic Sciences, McGill University, Montreal, Quebec, Canada

(Manuscript received 11 October 1995, in final form 19 January 1996)

ABSTRACT

Recent observations have revealed that some mesoscale convective systems (MCSs) could undergo multiple cycles of convective development and dissipation, and, under certain environments, they appeared to be responsible for (barotropic) oceanic or tropical cyclogenesis. In this study, oceanic cyclogenesis, as induced by an MCS moving offshore and then driven by deep convection in a near-barotropic environment, is investigated by extending to 90 h the previously documented 18-h simulation of the MCSs that were responsible for the July 1977 Johnstown flash flood. It is demonstrated that the mesoscale model can reproduce very well much of the meso-β-scale structures and evolution of the long-lived MCS out to 90 h. These include the development and dissipation of the continental MCSs as well as the associated surface and tropospheric perturbations, the timing and location in the initiation of a new MCS after 36 h and in the genesis of a surface mesolow over the warm Gulf Stream water after 60-h integration, the track and the deepening of the surface cyclone into a "tropical storm," the maintenance of a midlevel mesovortex/trough system, and the propagation of a large-scale cold front with respect to the surface cyclone.

It is found that the new MCS is triggered after the vortex/trough moved offshore and interacted with the land–ocean thermal contrasts during the afternoon hours. The oceanic cyclogenesis begins at 150–180 km to the south of the vortex, as the associated surface trough advances into the Gulf Stream and weakens. Then, the cyclone overpowers quickly the low-level portion of the vortex circulation and deepens 14 hPa in 24 h. A comparison with a dry sensitivity simulation shows that the cyclogenesis occurs entirely as a consequence of the convective forcing. Without it, an 84-h simulation produces only a surface trough with the minimum pressure being nearly the same as that left behind by the previous MCSs. It is shown that the vortex/trough provides persistent convergence at its southern periphery for the continued convective development, whereas the convectively enhanced low-level flow tends to (i) "pump" up sensible and latent heat fluxes from the warm ocean surface and (ii) transport the high-θ_e air in a slantwise fashion into the region having lower θ_e aloft, thereby causing further conditional instability, increased convection, and more rapid deepening. The interactions of the continental MCS/vortex and the oceanic cyclone/storm systems with their larger-scale environments are also discussed.

1. Introduction

Recent observations have shown that during the summer months, numerous mesoscale convective complexes (MCCs, Maddox 1980) in North America tend to form over the eastern slope of the Rocky Mountains (e.g., see annual MCC summaries by Maddox et al. 1982; Rodgers et al. 1983, 1985; Augustine and Howard 1988, 1991). Some of these MCCs can persist for several days as they move eastward across the continent. For example, Bosart and Sanders (1981, hereafter BS81) traced a mesoscale convective system (MCS), that was responsible for the Johnstown, Pennsylvania, flash flood of 19–20 July 1977, back to an origin in South Dakota 3 days earlier. Fritsch et al. (1994) examined the evolution of an MCS that formed in eastern Colorado and underwent five cycles of convective development and dissipation as it moved to southern Quebec over a period of 3 days. Cotton et al. (1983) and Wetzel et al. (1983) reported the development of 14 MCCs during an 8-day period in August 1977 with their initial convective roots near the Colorado Rockies. It is remarkable that *3 of the 14 MCCs* maintained their identity for as long as 3–5 days as they tracked toward the Atlantic Ocean along a weak quasi-stationary surface front. It appears that more of such long-lived MCSs,[1] occurring each year, have yet to be documented.

These long-lived MCSs seem to be a special class of organized mesoscale weather system during the summer months. The above-cited studies reveal that these

Corresponding author address: Dr. Da-Lin Zhang, Dept. of Atmospheric and Oceanic Sciences, McGill University, 805 Sherbrooke Street West, Montreal, Quebec H3A 2K6, Canada.
Email: dzhang@zephyr.meteo.mcgill.ca

[1] In the present study, a long-lived MCS is defined as the duration of its convective activity longer than a diurnal cycle (i.e., >24 h).

MCSs tend to be most intense and compact at night (the so-called nocturnal thunderstorm maximum, see Wallace 1975), and weak and loosely organized during the daytime. These systems can produce a variety of significant weather events during their lifetime, ranging from gust winds to severe thunderstorms and localized heavy rainfall. Their importance as major contributors to the warm-season rainfall over much of the midwestern United States has been documented by Fritsch et al. (1986) and McAnelly and Cotton (1989). Because of their longevity and intense latent heat release, these MCSs can greatly modify the environment in which they are embedded, for example, near the tropopause (e.g., Fritsch and Maddox 1981; Fritsch and Brown 1982), in the midtroposphere (e.g., Maddox 1983; Menard and Fritsch 1989; Cotton et al. 1989), and in the boundary layer (BS81; Fritsch et al. 1994). Therefore, long-lived MCSs present many challenges to the research and operational communities, which range from gaining insight into various physical processes and scale interactions to improving the operational forecasts of these weather systems and their associated precipitation.

Of particular relevance to this study is that some long-lived MCSs could induce by themselves (i.e., with little baroclinic forcing) intense mesocyclones or tropical storms, after they moved into warm water surfaces. The long-lived MCS to be investigated herein, that produced the 19–20 July 1977 Johnstown flash flood and later developed into a "tropical storm"[2] over the Atlantic Ocean (BS81), is one of the well-known examples. Recent studies of MCC populations around the world (e.g., Velasco and Fritsch 1987; Miller and Fritsch 1991; Laing and Fritsch 1993) showed numerous instances where tropical depressions or cyclones were generated from MCCs as they moved into warm oceans. In addition, it has been observed during TEXMEX[3] that some tropical cyclogenesis events appeared to evolve from MCSs as they moved offshore (Emanuel et al. 1993). However, little work has been done to examine the environmental conditions under which this type of cyclogenesis occurs, the processes leading to the cyclogenesis from MCSs, and the relationships between the genesis and deep convection. Several fundamental questions concerning the long-lived nature of MCSs and their subsequent transformation into tropical storms remain to be addressed. For example, under what environmental conditions will an MCS be longer lived? Is there any generic flow structure(s) of MCSs that may survive for more than a diurnal cycle? How could an MCS, often having a midlevel mesovortex,[4] evolve into an oceanic mesocyclone with intense cyclonic vorticity at the low levels? In a more specific term, what processes are responsible for the transformation of convectively generated cold pools in the lower troposphere (see Maddox 1983; Zhang and Fritsch 1987) to warm-core anomalies as oceanic cyclogenesis occurs (e.g., Gray 1979; Anthes 1982; Emanuel et al. 1993)?

There is increasing evidence to suggest that an MCS could become long-lived because of (i) the development of a midlevel mesovortex in the trailing stratiform region, and (ii) the presence of a weak-sheared environment in which the MCS/vortex is embedded (Zhang and Fritsch 1987, 1988a; Bartels and Maddox 1991; Fritsch et al. 1994). Specifically, when mesovortex circulations are sufficiently intense and balanced (Davis and Weisman 1994; Raymond 1992), they may become inertially stable so that the lifetime of the parent MCS could be lengthened (Schubert and Hack 1982; Zhang and Fritsch 1987, 1988a). When the midlevel mesovortex is embedded in a weak-sheared flow, its absolute vorticity is nearly conserved in the absence of friction. Additionally, the weak vertical wind shear and small horizontal deformation will slow down the ventilation of the mid-to-upper-level warm core and moist columns associated with mesovortices (Zhang and Fritsch 1987). In fact, some mesovortices have been reported to remain coherent for several days, playing an important role in triggering subsequent convective developments (e.g., Wetzel et al. 1983; Fritsch et al. 1994). However, it is still uncertain how midlevel mesovortices cause the multiple development of MCSs and oceanic cyclogenesis downstream.

This study is the first in a series of papers that address the aforementioned issues through the numerical investigation of the roles of the MCS/vortex associated with the 19–20 July 1977 Johnstown flood in the subsequent oceanic cyclogenesis. The objectives of the present paper are to (i) demonstrate the mesoscale predictability of the long-lived MCS from its MCS/vortex development over land to the oceanic development of a cyclone/storm system out to 90 h; (ii) examine the evolution of the mesovortex and its roles in the initiation and organization of the oceanic storm after 36 h into the integration; and (iii) determine the roles of deep convection versus large-scale forcing in the oceanic cyclogenesis, using the Penn State–National Center for Atmospheric Research (PSU–NCAR) mesoscale model. Zhang and Fritsch (1986, 1987), hereafter referred to as ZF86 and ZF87, respectively, have pre-

[2] The term "tropical storm," which was first used by BS81, is adopted here because the convectively generated flow structures and the environment in which the storm was embedded are similar in many aspects to those of tropical cyclones. One anonymous reviewer suggests the use of the term, "oceanic barotropic cyclone."

[3] Tropical Experiment in Mexico conducted between 1 July and 8 August 1991 (see Emanuel et al. 1993).

[4] A mesovortex is defined here as a closed wind circulation at a scale of greater than 150 km in diameter with its relative vorticity larger than that of the local Coriolis parameter f (see Zhang and Fritsch 1987).

sented a successful 18-h simulation of the squall line and MCC that were associated with the Johnstown flood events, as verified against the detailed analyses of Hoxit et al. (1978, hereafter H78) and BS81. The integration was terminated at 18 h because the model-simulated MCC and convectively generated circulations weakened rapidly thereafter. However, as documented by BS81, a surface trough left behind by the dissipated MCC appeared to "reintensify" to a closed mesolow 36 h after it drifted into the Atlantic Ocean. Then, the surface mesolow developed to tropical storm intensity in 24 h (i.e., at 0000 UTC 23 July) before it was overtaken by a large-scale cold-frontal system. Therefore, for the purpose of the present study, we utilize a much larger domain size to extend the previously documented 18-h integration of the case to 90 h, at which time the surface cyclone had reached tropical storm intensity. The dynamic and thermodynamic processes leading to the oceanic cyclogenesis and their vertical structures will be explored in Part II (Zhang and Bao 1996).

The next section describes briefly the major improvements and additions of the PSU–NCAR mesoscale model when applied to the simulation of the present long-lived MCSs. Section 3 provides verification of the 90-h simulation against BS81's surface analysis and other available observations, and presents the basic sequence leading to the development of the "tropical storm." The relative significance of convective versus large-scale forcings in the cyclogenesis will also be evaluated. Section 4 shows the simulated structure and evolution of a mesovortex, its associated short-wave trough and larger-scale flows in relation to the surface development. Section 5 discusses the mechanism(s) by which the oceanic storm is initiated as the dissipated MCC moves offshore, and then organized after 60 h into the model integration. A summary and concluding remarks are given in the final section.

2. Model description and initial conditions

The numerical model used in this study is an improved version of the PSU–NCAR three-dimensional, hydrostatic, nested-grid, mesoscale model (MM4, see Anthes et al. 1987), which is similar to that used by ZF86, Zhang et al. (1988) and Zhang (1989) for the 18-h simulation of the same case. The fundamental features of the model used for this study include (i) a two-way interactive nested-grid procedure that allows incorporation of realistic topography (Zhang et al. 1986); (ii) an explicit moisture scheme containing prognostic equations for cloud water (ice) and rainwater (snow) (Hsie et al. 1984; Zhang 1989; Dudhia 1989); (iii) the Blackadar boundary layer parameterization scheme (Zhang and Anthes 1982); and (iv) the specification of the coarse-mesh outermost lateral boundary conditions by linearly interpolating 12-h observations according to Perkey and Kreitzberg (1976).

a. Model improvements

While the basic model framework is the same as that used in ZF86 and Zhang (1989), there are a few important additions and improvements that have been incorporated in order to obtain realistic simulations of long-lived MCSs. First, the Kain-Fritsch (1990, 1993, hereafter KF) convective parameterization scheme is used instead of the Fritsch–Chappell (1980) scheme for the fine-mesh portion of the model in order to minimize the differences between subgrid-scale and grid-scale moist physics representations (Molinari and Dudek 1992; Zhang et al. 1994), while for the coarse mesh the Anthes–Kuo (Anthes et al. 1987) scheme is still utilized. The KF scheme is based upon the same closure assumptions as the Fritsch–Chappell scheme, but uses a cloud model that is designed to allow updraft entrainment and detrainment rates to vary more realistically as a function of environmental conditions. In particular, the latest version of the KF scheme allows the direct feedback of both vapor and hydrometeors to the grid scale, thereby eliminating the uncertainty associated with the sedimentation process in the Fritsch–Chappell scheme (see Zhang et al. 1994). The coupling of the KF scheme with the explicit moisture scheme tends to help reproduce different types of mesoscale precipitating systems (Zhang et al. 1988; Molinari and Dudek 1992).

Second, an improved version of the Garand (1983) broadband infrared radiation scheme is adopted to account for the effect of persistent cloudiness associated with the long-lived MCSs under investigation. The Garand radiation scheme includes water vapor line and continuum absorption, clouds, carbon dioxide, and ozone with tabulated transmission functions based on the HITRAN (Rothman et al. 1987) spectroscopic databank. This version of the scheme is very similar to that used in the operational version of the Canadian regional finite-element model (Benoit et al. 1989), except that cloud amount is defined here in accordance to the model-predicted grid-scale cloud water (ice) and rainwater (snow) instead of relative humidity. The scheme is computed every 30 min and it costs less than 5% of total CPUs due to the use of the tabulated database. Krishnamurti et al. (1991), Kurihara and Tuleya (1981), and others have documented the importance of including longwave radiative transfer in obtaining realistic simulations of tropical storms.

Third, because the long-lived MCSs under study traverse a great distance during the 90-h period (see Fig. 1), a simple grid-moving strategy is developed to reduce the storage and computational costs. In this strategy, the fine-grid mesh can be moved at the times and speeds as specified. A shift of the nested-grid mesh is achieved by changing coarse-mesh points at the leading side to fine-mesh points and fine-mesh points at the trailing side to coarse-mesh points. All prognostic variables in the newly formed coarse- and fine-mesh

regions are obtained by nine-point averaging and interpolation, respectively. Special care has been taken to ensure the consistency of topography (Zhang et al. 1986) and surface parameters for each shift of the nested-grid mesh.

Fourth, the geographic distribution of the surface parameters, that is, moisture availability, roughness, albedo, and thermal inertial, which determine surface energy budgets and the development of the planetary boundary layer (PBL), is derived from the land-use data archived at NCAR using MM4's standard processing programs, rather than specified as that in ZF86.

The nested-grid ratio is 1:3 with a fine-mesh length of 25 km and a coarse-mesh length of 75 km. The (x, y, σ) dimensions of the coarse and fine meshes are 59 $\times$ 45 $\times$ 19 and 85 $\times$ 49 $\times$ 19, respectively. The vertical terrain-following coordinate σ is defined as $\sigma = (p - p_t)(p_s - p_t)^{-1}$, where p_t is the pressure at the model top (in this case 70 hPa) and p_s is the surface pressure. Figures 1 and 2 show the fine-mesh (at the initial time) and coarse-mesh domains, respectively (whereas the fine-mesh domain after 60-h integration is given in Fig. 16). See Anthes et al. (1987), ZF86, Zhang et al. (1988), and Zhang (1989) for other details of the model being used.

b. *Initial conditions*

The nested-grid model is initialized at 1200 UTC 19 July 1977 using the same dataset and same procedures as those described by ZF86, and then integrated to 90 h. The model initial conditions at 700 hPa and the surface are given in Fig. 2. Sea surface temperatures (SST) are also plotted, which are derived from the National Meteorological Center (NMC, now referred to as the National Centers for Environmental Prediction) global analysis and enhanced by ship reports and buoy data. One can see that most of the eastern United States

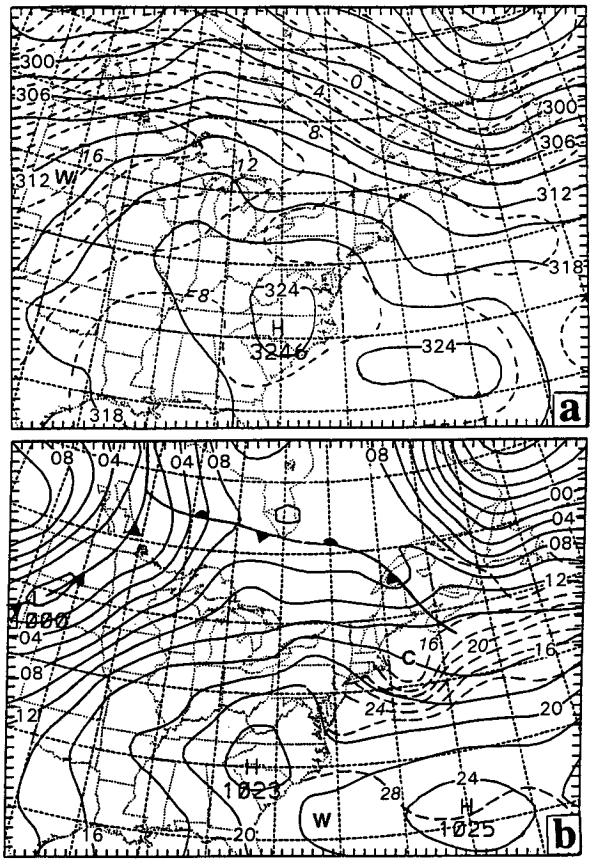

FIG. 2. Model initial conditions over the coarse-mesh domain at 1200 UTC 19 July 1977. (a) Geopotential heights (solid) at intervals of 3 dam and temperature (dashed) at intervals of 2°C at 700 hPa. (b) Sea level pressures at intervals of 2 hPa, labeled as the excess over 1000 hPa, e.g., "08" = 1008 hPa; similarly for the rest of figures. Dashed lines denote sea level temperature at intervals of 2°C. The intervals marked on the frame are mesh grids (75 km for coarse mesh; similarly in the rest of figures).

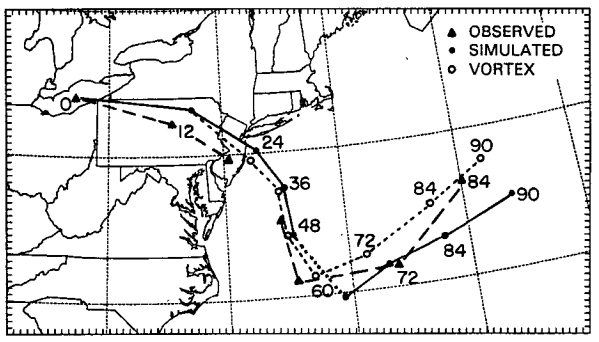

FIG. 1. Comparison of the tracks of the observed surface mesolow (long dashed) with the model-simulated (solid) over the fine-mesh domain. Dotted portion of the simulated track indicates the dissipation of the previous mesolow and the formation of a new mesolow. The path of the 700-hPa vortex center is also given (short dashed). The intervals marked on the frame are mesh grids (25 km for fine mesh; similarly in the rest of figures).

is under general anticyclonic flow around a quasi-stationary subtropical high centered in the western Atlantic. Because of this flow structure, there is a continuous flow of warm and moist air into the mid-Atlantic states (see H78; ZF86). A sea level pressure trough associated with a short-wave trough aloft, which is evident over the Great Lakes region, is superposed on the large-scale (subtropical) ridge. BS81 showed that this mesoscale disturbance has propagated with the MCSs since its initiation in South Dakota 3 days earlier. Associated with the short-wave trough is a nearly balanced vortex circulation in the midtroposphere (see ZF86 and ZF87). As will be seen later, this trough/vortex system also moves eastward at the same speed as the surface trough (or later mesolow) during the subsequent 90 h. Evidently, this trough system plays an important role in inducing favorable upward motion for the initiation of new convection over Lake Erie at the

model initial time (see ZF86). To the west of the trough, strong warm advection occurs in the lowest 300–400 hPa (Fig. 2a), and it decreases rapidly upward (see BS81 and ZF86). Farther to the north is strong baroclinicity associated with a large-scale frontal system that extends from central Canada into the northern high plains of the United States. It is this cold front that will catch up with the oceanic cyclone near the end of the 90-h integration. As Zhang and Fritsch (1988b) demonstrated with a series of sensitivity simulations, this frontal system provides a favorable environment for the development of the MCSs, but its forcing is too remote to determine the structure and evolution of the MCSs during the first 18-h integration.

3. Numerical simulations

In this section, we document the sequence of events from the initial convective development over land to the final "tropical storm" stage over ocean, and verify the 90-h simulation against available observations. ZF86 have shown that the first 18-h model integration reproduces many of the different aspects of the MCC and squall line that were responsible for the heavy rain over western Pennsylvania. These include the development of surface mesohighs, mesolows, and outflow boundaries, the propagation of mesoscale gravity waves and the evolution of a midlevel short-wave trough and a mesovortex, as verified against detailed observational analyses by H78 and BS81. By 0600 UTC 20 July (i.e., 18 h into the integration), henceforth 20/06-18, the MCSs have dropped substantial rainfall over the Johnstown area and begun to dissipate quickly hereafter (see Fig. 3a). The MCSs left behind two surface mesohighs, that is, one over eastern Pennsylvania and the other over the west central portion of the state, with a surface mesolow in between (see Fig. 4). Note that this surface mesolow was located in the trailing stratiform region to the north of the convective line. The mesolow was maintained for at least another 3 h as the MCC moved southeastward and dissipated, and then it weakened to a mesotrough (see H78). The evolution of the surface mesolow (or trough) in relation to the midlevel trough/mesovortex system is of particular relevance to the present study. Since H78, BS81, and ZF86 have discussed extensively the life cycle of the MCSs up to 20/06-18, we will focus mainly on the evolution of the system during the subsequent 72 h and identify the sequences leading to the eventual tropical-storm intensity.

Figures 1 and 5 compare, respectively, the tracks and central pressures of the simulated and observed surface mesolows. Because of the absence of significant signals during the system's dissipation stage, the central value and position of the surface low at 21/00-36 could not be identified from the BS81 analysis. Even so, it is still possible to see that the surface pressure center as well as the midlevel mesovortex moved first southeastward under the influence of anticyclonic flow associated with the subtropical high (see Fig. 2a), and then an abrupt changeover to northeastward displacement occurred after 22/00-60. One can also see that the system's forward movement slowed after it moved offshore, (i.e., <4 m s^{-1} vs. 6–8 m s^{-1} during the previous 24 h), and it accelerated to a speed of more than 9 m s^{-1} as the system rapidly deepened. Note that the oceanic cyclogenesis occurs at the south periphery of the trough/vortex (or "dissipated" low) at 22/00–60, thus causing a "jump" in the positions of the surface lows between the 48- and 60-h simulations. In general, the model reproduces well the basic track of the surface mesolows, particularly the directional change, although the dissipated low is simulated to move a little faster and the "new" low slower than the observed (see Fig. 1). Likewise, the model reproduces well the dissipation rate of the "old" low after the Johnstown flooding episodes and the deepening of the "new" mesolow shortly after 21/12-48 (Fig. 5). At the end of the 84-h integration, the model-simulated cyclone is identical in intensity to the observed but its center departs about 200 km from the analyzed (Figs. 1 and 5). The difference in position, as will be shown, is mainly due to the use of different parameters to define the cyclone center in the BS81 analysis and the simulation. The results are very encouraging since the simulation of convectively generated mesoscale circulations out to 84 h greatly exceeds the predictability limits indicated by traditional predictability concepts (see Anthes and Baumhefner 1984; Stull 1985).

Our analysis of the cyclogenesis events begins by examining closely how well the model reproduces mesoscale and larger-scale circulations in a subdomain framework. As mentioned previously, the surface pressure perturbations weaken rapidly as the MCC dissipates. At 20/12-24, both the simulation and BS81's analysis show only a weak surface trough near the east coast in association with the dissipating MCC (see Fig. 9 in BS81 and Fig. 6 herein). Although remnant showers and thunderstorms continued in the lee of the Appalachians (see BS81 and Fig. 3a), the model convection over the region has disappeared during the late night hours. However, the model reproduces a line of remnant convection ahead of the surface trough, which, to be shown in section 5, results from convectively generated cold outflow interacting with conditionally unstable environment ahead. The line continues to propagate eastward, in a density current fashion, during the next 12 h, as indicated by the letter "D" in Figs. 3a, 3b, 6, and 7b. The simulated pressure perturbations associated with the convective line can also be inferred from surface wind reports in the BS81 analysis (see Fig. 7a).

At 21/00-36, the satellite imagery shows much less cloudiness associated with the dissipated MCC, and arc-shaped shallow cloudiness to the south that oc-

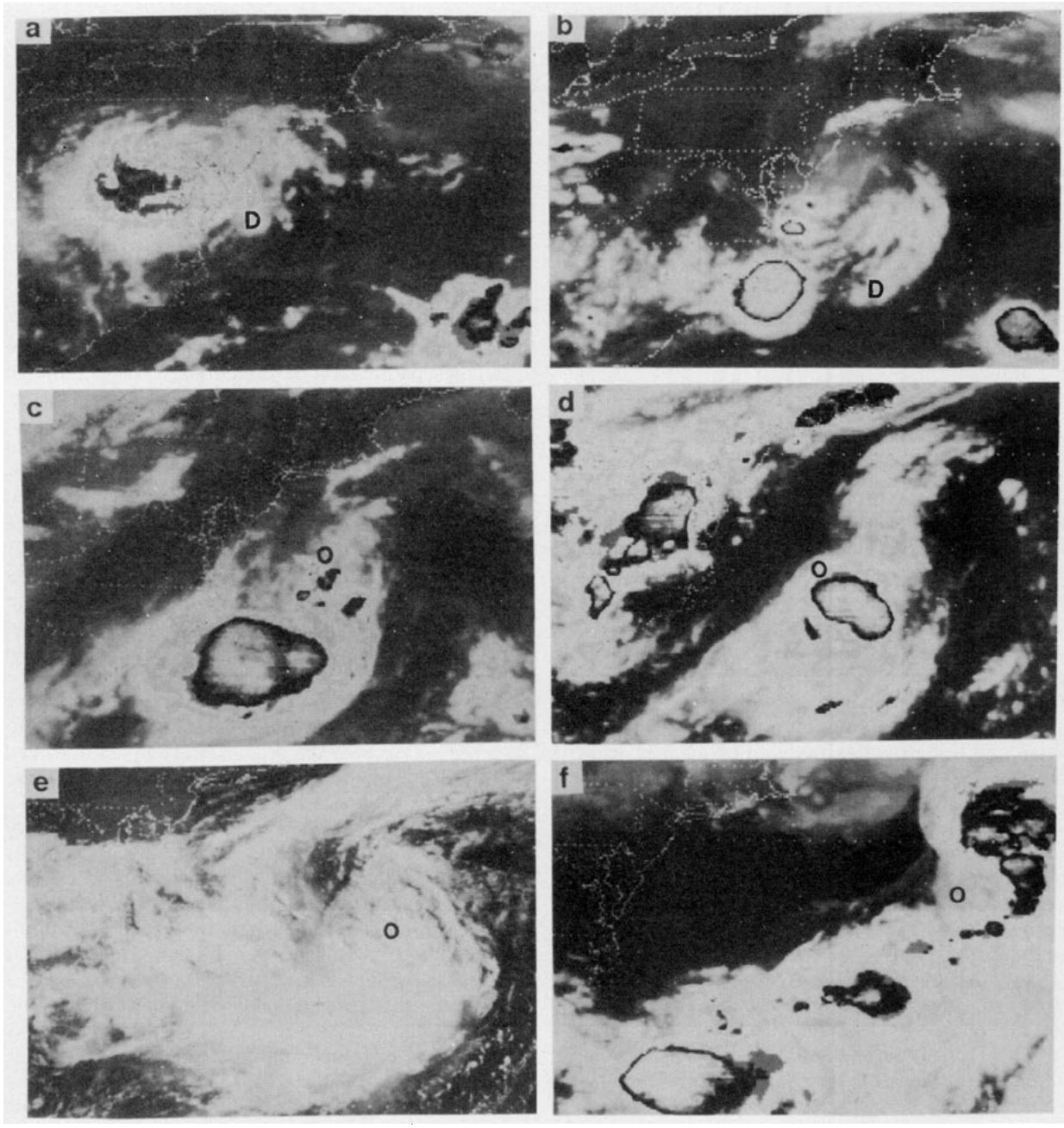

FIG. 3. *GOES-1* visible and infrared satellite imagery for (a) 1200 UTC 20, (b) 0001 UTC 21, (c) 1200 UTC 21, (d) 0001 UTC 22, (e) 1230 UTC 22, and (f) 0001 UTC 23 July 1977. Letters "D" and "o" denote the distribution of a line convection along a cold outflow boundary and the location of the surface cyclone center from the BS81 analysis, respectively.

curred along the outflow boundary of the system (see Fig. 3b). Meanwhile, both the BS81 analysis and the 36-h integration display the continued weakening of the convectively generated surface pressure perturbations; their pertinent signals are almost indiscernible at this time (Fig. 7). Of importance is that an intense convective system emerged at the southern periphery of the dissipated MCC, that is, near the North Carolina coast. Interestingly, the model also captures the development of such a convective system at nearly the right time and right location. As will be shown in section 5, this new MCS is triggered as a consequence of the mesovortex circulations interacting with the land–ocean thermal contrasts during the early afternoon hours. For a similar

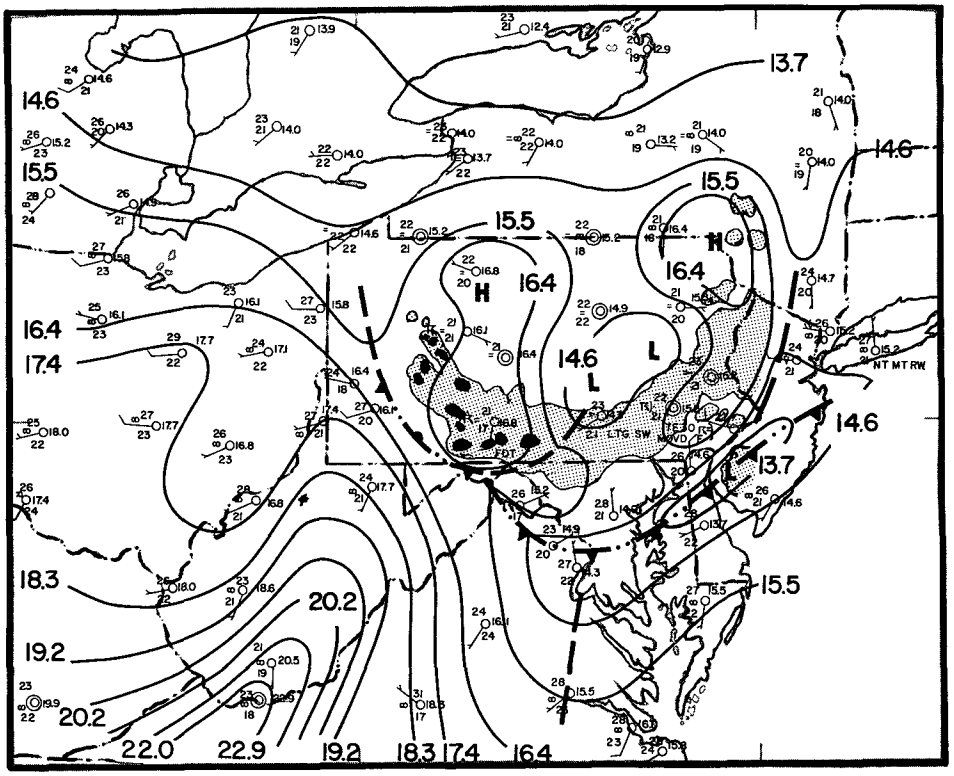

FIG. 4. Surface analysis for 0600 UTC 20 July 1977 (adapted from H78). Frontal symbols alternated with double dots indicate moist-downdraft outflow boundaries. The light shading denotes the level 1 radar echoes and the dark shading denotes level 3 (or greater) radar echoes. A full wind barb is 5 m s^{-1}.

reason, the model appears to reproduce a few isolated, though aliased, deep convection off the Virginia coast. It can be seen from Figs. 3b–f that this new MCS expanded rapidly as it drifted eastward over the warm ocean surface (Fig. 2b). Later it became the dominant cloud system contributing to the deepening of the surface cyclone. For the sake of subsequent discussions, the dissipated and newly formed MCSs will be hereafter referred to as the continental and oceanic (or convective band) storms, respectively, although the latter

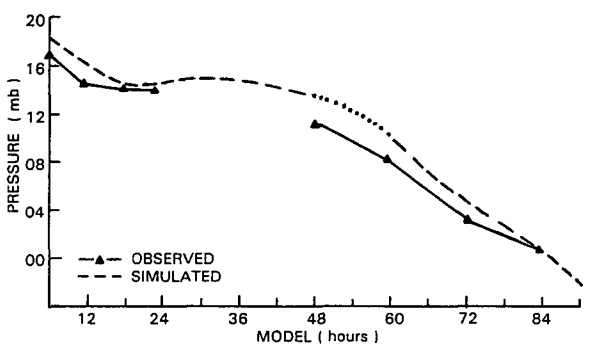

FIG. 5. Comparison of the observed (solid) and simulated (dashed) central pressures of the surface cyclone as a function of the model integration time. Dotted portion of the pressure trace indicates the dissipation of the previous mesolow and the formation of a new mesolow.

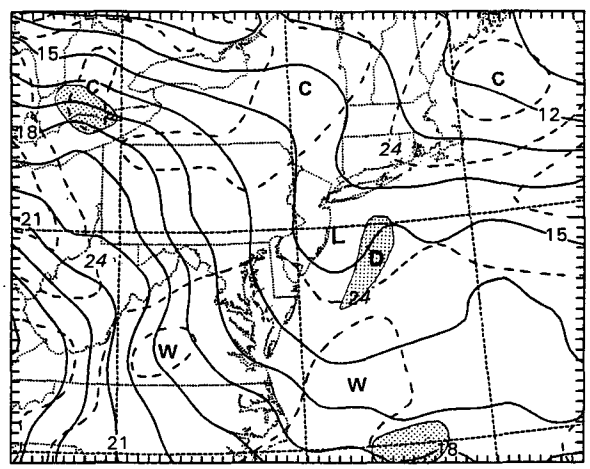

FIG. 6. Analysis of sea level pressure (solid, every 1 hPa) and surface temperature (dashed, every 2°C) over a fine-mesh subdomain from 24-h integration (20/12-24). Shading denotes the area of active model convection at the hour. Letter "D" denotes the distribution of a line convection along a cold outflow boundary.

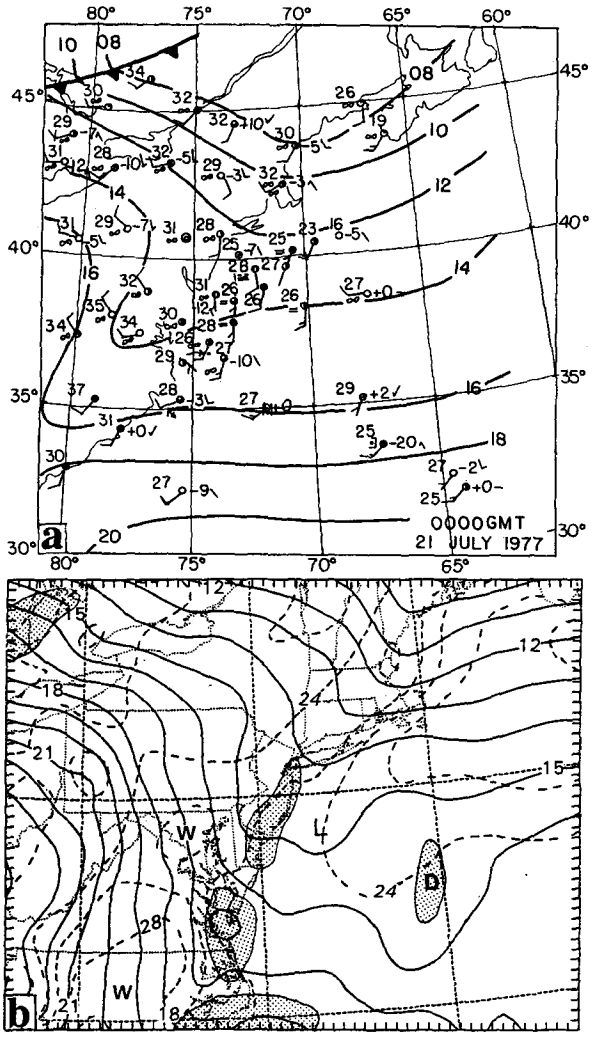

FIG. 7. (a) Surface analysis for 0000 UTC 21 July 1977 (adapted from BS81). Sea level pressure is contoured at every 2 hPa. A full wind barb is 5 m s^{-1}. (b) As in Fig. 6 but from 36-h integration (21/00-36).

could be regarded as the revival of the previously dissipated MCC.

Although the model reproduces most of the significant meteorological features, there are several notable deficiencies. For example, the model appears to have overproduced the intensity of the subtropical high by 2–4 hPa, as compared to the H78 and BS81 analyses. As a result, the low-level winds over the region tend to be overpredicted (cf. Figs. 8a and 8c). The simulated intensity of the subtropical high is in better agreement with the analyzed when the Garand radiation scheme was turned off, like that shown in ZF86, suggesting that this overproduction results partly from excessive longwave cooling in the free atmosphere. The generation of an anomalously strong subtropical high appears to have pushed the surface trough (or midlevel mesovortex) a

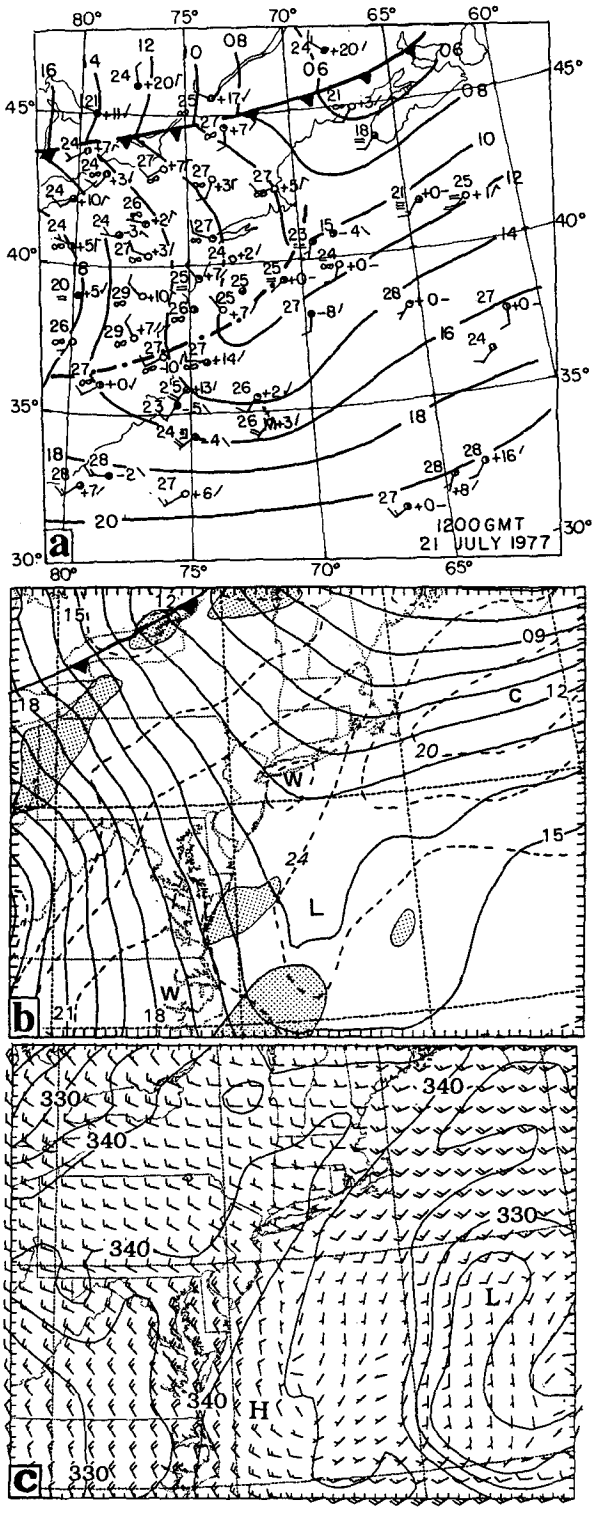

FIG. 8. (a) Surface analysis for 1200 UTC 21 July 1977 (adapted from BS81). Sea level pressure is contoured at every 2 hPa. (b) As in Fig. 6 but from 48-h integration (21/12-48). The frontal position is specified according to θ_e at 900 hPa (see text). (c) Analysis of surface winds and 900-hPa θ_e (solid) at 5-K intervals from 48-h integration. Winds plotted according to convention with each pennant, full barb, and half barb denoting 25, 5, and 2.5 m s^{-1}, respectively.

little too far to the southeast at 21/12-48 and 22/00-60, as compared to the BS81 analysis (see Fig. 1).

The oceanic storm continued to expand and intensify at night, and by 21/12-48, it developed into an MCC type of system (see Fig. 3c). Very encouragingly, the model reproduces reasonably well the continued expansion of the new convective system during the evening hours (Fig. 8). Evidently, the MCS of this size begins to exert an important influence on the subsequent evolution of the surface pressure perturbations. However, its influence is still not visible in the BS81 analysis. This may be attributable to the relatively poor density of observations offshore. In contrast, the 48-h integration shows a sign of consolidation of the surface pressure perturbations into a deeper mesotrough as the system moves southeastward to lower latitudes under the anticyclonic influence (Fig. 8b). Meanwhile, the southwesterly flow ahead of the trough helps transport tropical high-θ_e air into the region for subsequent convective development. Thus, this period may be considered as the onset of the surface cyclonic development.

Also at this time, a large-scale cold front, located about 600–700 km to the northwest of the trough, rapidly approaches. The model appears to reproduce well some isolated convective systems along the cold front (cf. Figs. 3c and 8b). It should be mentioned that a moist isentrope (i.e., θ_e) of 335 K at 900 hPa in conjunction with surface winds is used to determine the position of the cold front. This definition differs from that used in BS81's surface analysis. As will be seen later, this definition provides a better description of the frontal position, particularly the continuity of the frontal evolution, as the cold front moves over the warm ocean surface. This is because θ_e is a conserved variable in an inviscid, pseudoadiabatic flow.

At 22/00-60, the BS81 analysis shows the generation of a closed surface mesolow or cyclone[5] just slightly to the northwest of the oceanic storm (cf. Figs. 9a and 3d). (The cloud shields to the north seen in Fig. 3d were still associated with the dissipated MCC.) It is promising that the model captures reasonably well the timing and the location of the surface intensification, *even after 60 h into the integration* (see Fig. 9b); the difference in position from the BS81 analyzed is about 150 km too far to the southeast. The model also reproduces an area of weak-gradient mass to the north of the mesolow, as a result of the continued weakening of the low-level circulation associated with the trough/vortex system. In other words, the surface mesolow develops *at the south periphery of rather than directly from the previous surface mesotrough or vortex,* which is consistent with the "jump" in the positions of the surface lows between the 48- and 60-h simulations (see Fig.

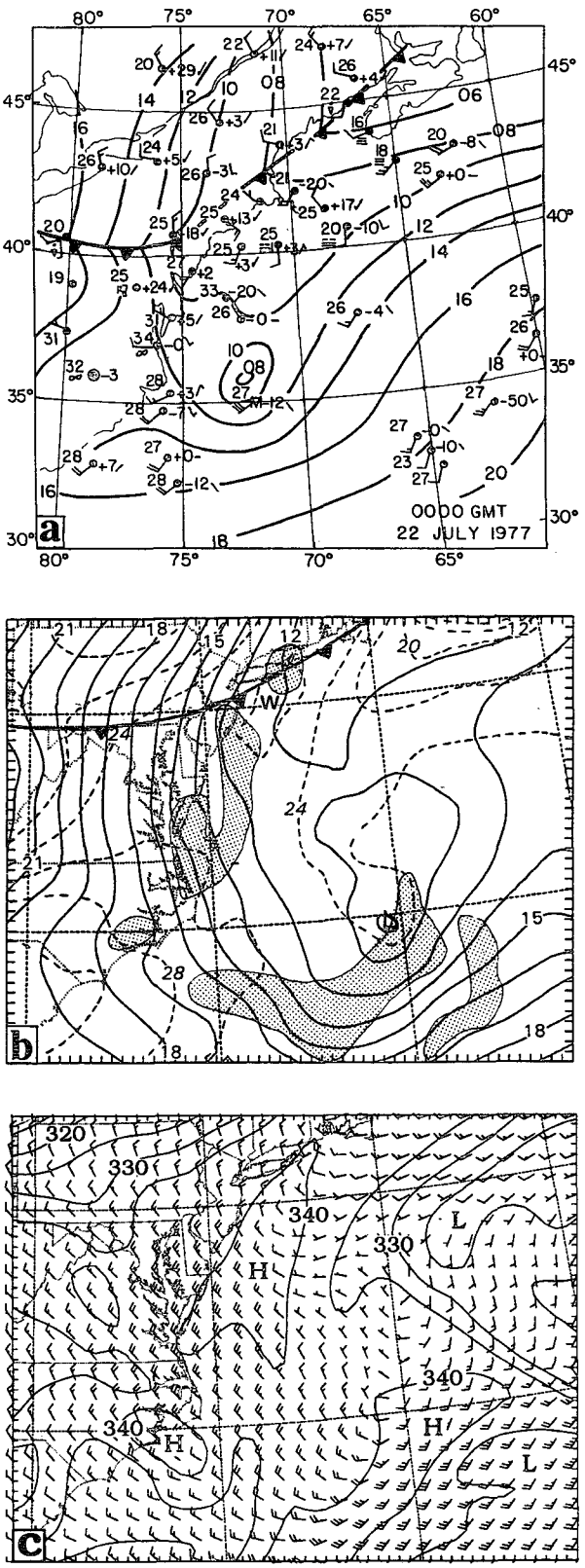

FIG. 9. As in Fig. 8 but for 0000 UTC 22 July 1977 and 60-h integration (i.e., at 22/00-60).

[5] Note that the "cyclone" or "mesolow" is used herein to denote closed wind circulations or isobars, which is distinguished from the oceanic storm or convective band.

1). The model-simulated MCS intensifies and expands into an elongated convective band[6] that is hugging the surface mesolow (cf. Figs. 9b and 3d). Furthermore, surface pressure gradients as well as surface winds along the oceanic storm have strengthened substantially during the previous 12 h (cf. Figs. 8c and 9c).

It is important to notice that all the above scenarios occur as the mesoscale disturbance moves to the *warm Gulf Stream water* (see Fig. 2b), where the air–sea temperature differences (in the lowest 15-m layer) range from −1.5°C at its ambient to about −3°C beneath the convective band (due to downdraft cooling) at 22/00-60. Figure 10 shows the relative magnitudes of surface sensible and latent heat fluxes at this incipient stage. It is seen that large positive fluxes occur in the vicinity of the storm, more pronounced along the intensifying southwesterly flow with an average Bowen ratio of 0.2. The sensible heat flux has a magnitude similar to that found by Black and Holland (1995) in Tropical Cyclone Kerry (1979), whereas the latent heat flux is only one-third to one-quarter of that in Kerry (1979). Because of the parameterized moist downdraft effects, a zone of enhanced sensible heat flux coincides with the convective band or intense surface flow, but it is not the case with the latent heat flux (due to near-saturated downdrafts conditions). Several TOGA COARE[7] analyses have also found the increased sea–air thermal fluxes in the vicinity of MCSs due to the presence of anomalously cool, dry, and windy downdraft currents in the PBL (see Parsons et al. 1994; Mapes and Houze 1995). Thus, the result suggests that strong surface winds will enhance (i) the upward transfer of heat and moisture fluxes from the warm water surface, and (ii) the transport of high-θ_e air in the PBL along the southwesterly jetlike flow into the region having lower θ_e aloft. These processes, enhanced by the convectively induced grid-scale transport, appear to play an important role in generating a low-level high-θ_e tongue along the convective band, which in turn tends to destabilize atmospheric columns, especially near the leading portion of the tongue, thereby assisting the further organization of the oceanic storm along the surface jetlike flow (Figs. 9b,c).

After 22/00-60, the surface cyclone spins up rapidly and overpowers the low-level circulations associated with the trough/vortex system. By 22/12-72, its central pressure has deepened from 1008 to 1003 hPa, that is, 5 hPa in 12 h (see Fig. 11a). It is evident that the model

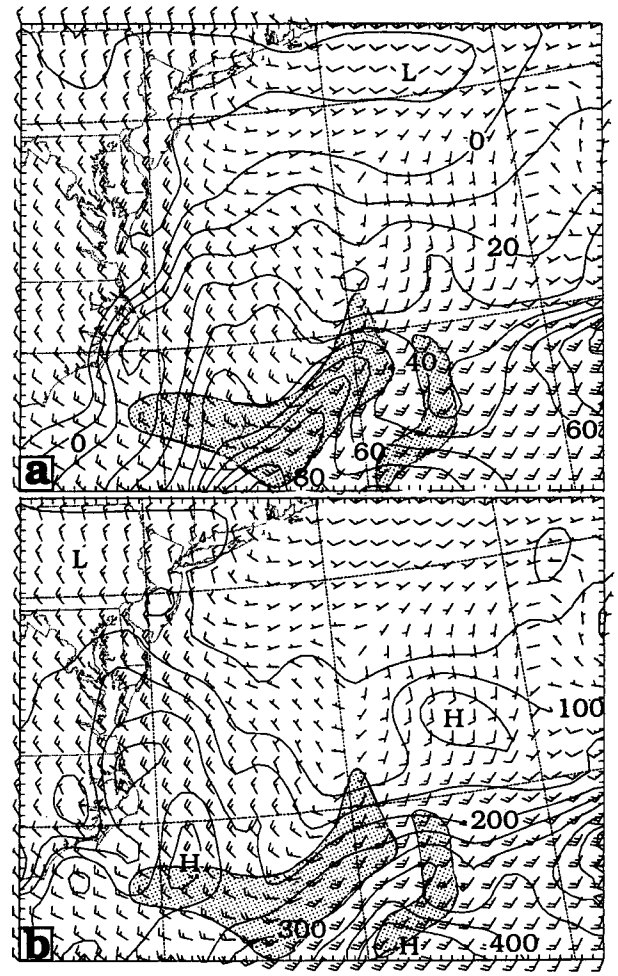

FIG. 10. Simulated surface (a) sensible heat flux at intervals of 10 W m^{-2} and (b) latent heat flux at intervals of 50 W m^{-2}, superposed with surface winds at 22/00-60. A full barb is 5 m s^{-1}. Shading denotes the distribution of the oceanic storm (see Fig. 9).

reproduces closely the intensity and location of the surface mesolow at this time (cf. Figs. 11a,b). Similarly, the model reproduces well the continued expansion of the oceanic storm to the south and southeast of the surface mesolow (cf. Figs. 3e and 11b), as well as the cloud activity along the cold front. The simulated pressure trough in the wake of the storm conforms to the reported surface pressure falls in the BS81 analysis. We will see in Part II that this represents part of the contribution of the vortex/trough system to the cyclogenesis, as the weak-gradient air mass is wrapped around cyclonically (cf. Figs. 9b,c and 11b,c). Rapid intensification of the surface flow also takes place during the 24-h period. For example, the southerly surface winds ahead of the cyclone, which were never more than 5 m s^{-1} at 48 h, increase to more than 15 m s^{-1} by 72 h (cf. Figs. 8c and 11c). As a result of the deepening, a closed cyclonic circulation formed ahead of the cold front, with enhanced

[6] In general, the model-produced convective distribution should be verified against radar observations, particularly after extensive anvil clouds developed. Unfortunately, radar observations for the present study were not available. Thus, we can verify only the simulated convective development against the satellite imagery.

[7] The Tropical Ocean Global Atmosphere program's Coupled Ocean–Atmosphere Response Experiment (see Webster and Lukas 1992).

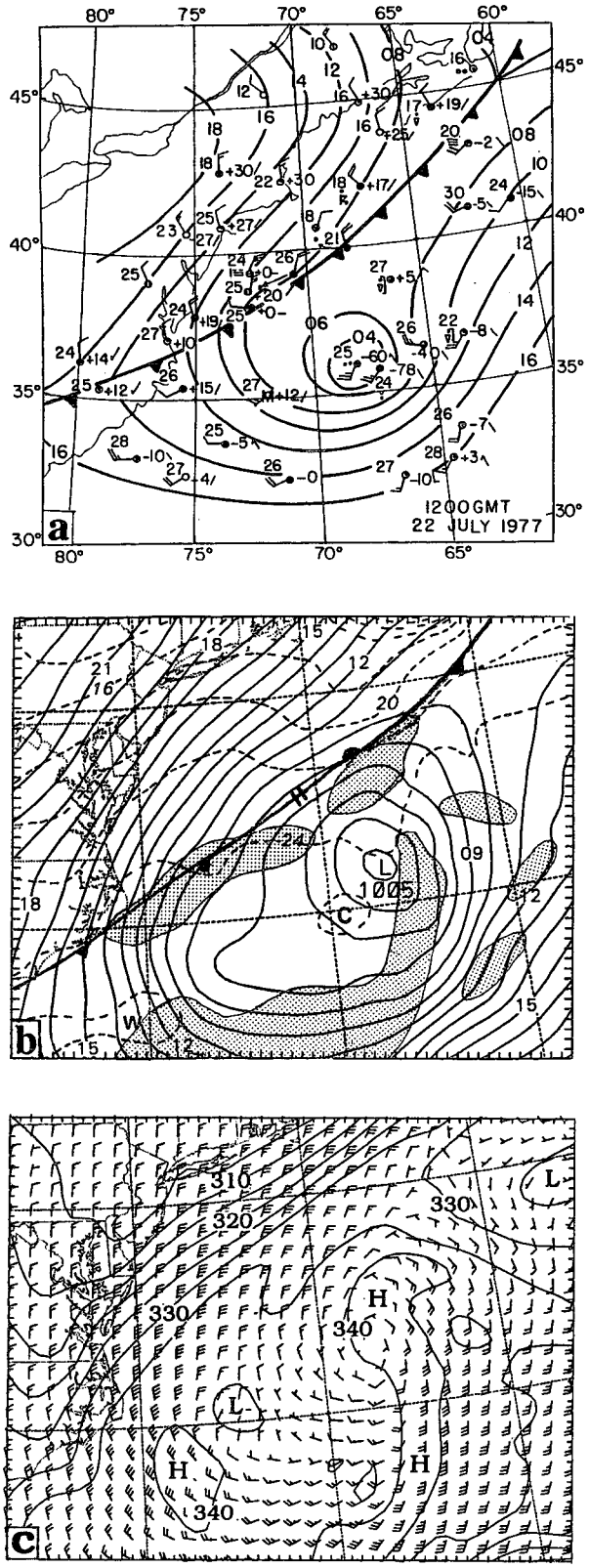

FIG. 11. As in Fig. 8 but for 1200 UTC 22 July 1977 and 72-h integration (22/12-72).

northward transport of high-θ_e air and more intense convective activity occurring in its southwest-to-southerly currents. Note the accelerations of surface flow as air parcels move from the land to water surfaces and the presence of strong θ_e gradients behind the cold front (see Figs. 9c and 11c). The model appears to underpredict the southwestern portion of the surface trough over the continent (cf. Figs. 11a–c). Note also that there is little wind shift across the frontal zone, particularly over the region between the front and surface mesolow. The near-90° cross-isobaric wind off the North Carolina coast in the BS81 analysis appeared to be a reflection of a smaller-scale circulation associated with the convective storm.

Of particular interest is that the weakest flow and little convective activity occur near the center of the simulated cyclone (see Figs. 11b,c). The simulated light winds at the cyclone center are consistent with those observed during the incipient stages of tropical cyclones (see Zehr 1992). An upper-air sounding, taken at the model cyclone center (see Fig. 12), shows a near-saturated condition in the lowest 50 hPa and a deep dry atmosphere aloft. This suggests that the air near the cyclone center has been descending (or descended), which is qualitatively in agreement with that which occurred in tropical storms (Anthes 1982). (The near-saturated but dry-adiabatic boundary layer, which results from the parameterized surface fluxes and advection of heat and moisture, suggests the necessity to include a shallow convection scheme to remove the local conditional instability.) However, one may note from the BS81 analysis that stronger winds (>12 m s^{-1}) were placed near the cyclone center (Fig. 11a). The different wind speeds from the BS81 analysis could be again attributed to the lack of high-resolution observations, particularly over this region, which is far offshore. It is also possible that the observed intense winds result from convective-scale motions, as suggested by another strong ageostrophic wind report to the east of the low (see Fig. 11a).

By 23/00-84, the surface mesolow has deepened another 4 hPa to 1001 hPa (see Fig. 13a). Meanwhile, surface winds at some distance to the southeast of the

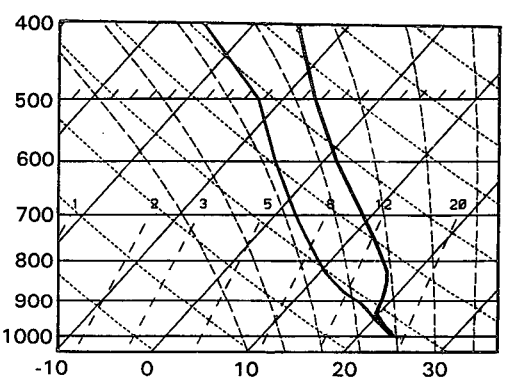

FIG. 12. Simulated upper-air sounding taken at the surface cyclone center at 22/12-72.

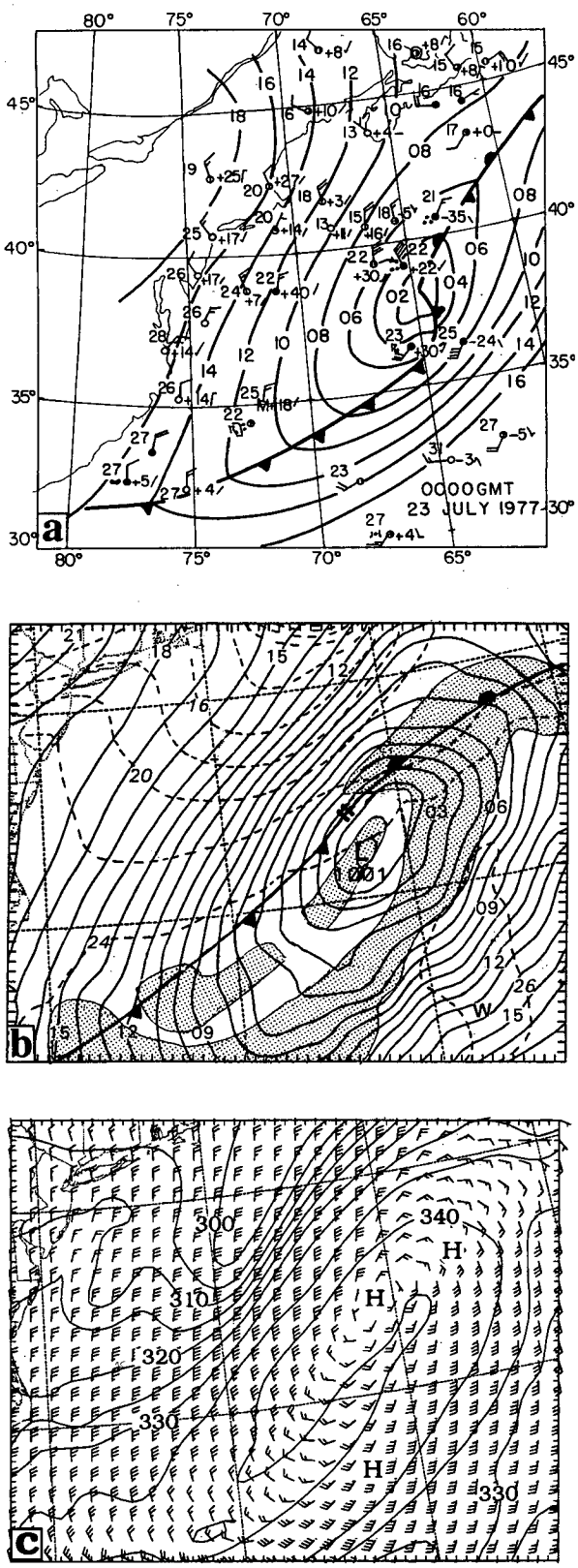

FIG. 13. As in Fig. 8 but for 0000 UTC 23 July 1977 and 84-h integration (23/00-84).

cyclone center have increased to over 20 m s^{-1}, thus reaching "tropical storm" intensity (see BS81; Gray 1979; Burpee 1986). It is encouraging that the model reproduces very well the intensity and location of the surface cyclone. The error in the position of the surface mesolow is less than 200 km. This error is very small, considering that this is the 84th-hour simulation of an MCS in a weak-gradient environment. It should be noted, however, that the center of the surface mesolow differs from that of the surface wind circulation (cf. Figs. 13b,c). The latter has frequently been used by mesoscale analysists to place the center of a surface low when reliable surface pressure observations were lacking, like in the present case (see Fig. 13a). Thus, the error in position is negligible when the closed wind circulation is compared to the BS81 analysis. In fact, as will be shown in Part II, the surface mesolow tends to be driven by a vorticity center (i.e., the wind field). Similarly, the model reproduces the larger-scale pressure pattern as well as the surface temperature distribution both ahead of and behind the surface front. Because of the cyclonic development, the northern portion of the surface front exhibits overrunning of high-θ_e air, which is characteristic of warm-frontal circulations (Figs. 11 and 13). One may note, nonetheless, that the BS81 analysis shows the merging of the cold front with the surface cyclone and associated broad trough to the southwest, whereas our 900-hPa θ_e analysis still indicates separation of the two systems at this hour. On the other hand, the two analyses would be consistent when the frontal positions are all specified along the axes of the broad troughs. We believe that our analysis provides a better depiction of the frontal position, since (i) there is a clear sign of strong θ_e gradients behind the front; and (ii) the broad trough ahead of the front is linked to the midlevel trough/vortex rather than the large-scale baroclinic trough, and it has been enhanced markedly by the development of the oceanic storm during the previous 24 h (see Figs. 9b, 11b, 13b, and 14).

It is also encouraging that the model reproduces the observed southerly and northerly surface jetlike flows with winds greater than 20 m s^{-1} symmetric about the cyclone center (see Fig. 13c). Associated with the two jetlike flows are the high- and low-θ_e tongues from different energy source regions. It is important to note from Figs. 9c, 11c, 13c how the high-θ_e air, resulted from the air–sea interaction (Emanuel 1986; Rotunno and Emanuel 1987), wraps around toward the cyclone center during the 24-h period. Because the high-θ_e tongue is closely related to the convective development with intense upward motion (cf. Figs. 11b,c and 13b,c), its wrapping-around tends to occur in a slantwise fashion.[8] A similar wrapping-around scenario has

[8] Note that the cyclonic-slantwise wrapping, which is more significant along the convective band, is described herein in a volume-

also been noted by Ryan et al. (1992) in their analysis of a wide rainband associated with a developing tropical cyclone. In the present case, it can also be inferred from the low-level spiral cloudiness in the satellite imagery (e.g., Fig. 3e). By 23/00-84, the leading portion of the high-θ_e tongue has entered into the northerly return flow ahead of the cold front, thus forming a "comma-shaped" high-θ_e tongue. This appearance of the tropical high-θ_e air in the northerly return flow further suggests that the frontal and the cyclone systems have not been merged at this stage. Likewise, the model simulates well the basic pattern of deep convection, particularly the "comma" head to the northeast of the cyclone (cf. Figs. 3f and 13b). A comparison of the satellite imagery with the BS81 analysis reveals that the cyclone center (i.e., the point, "o," in Fig. 3f) was located to the southwest of the "comma" head, that is, the region with low-level stratiform clouds. This further reveals the development of descending (or weak vertical) motion over the cyclone center, at least in the middle to upper troposphere, and provides an indirect validation of the sounding given in Fig. 12. The simulated cyclone center is also situated to the southwest of the "comma" head.

At this point, one may argue that the distributions of surface pressure and wind fields, as well as convective development relative to the cyclone, are no different than those in typical extratropical (baroclinically driven) cyclones. First, we have shown that the present cyclone develops in a weak-gradient, prefrontal environment (see Figs. 2 and 18). Second, we will see in Part II (Figs. 4–6) that the cyclone exhibits in the vertical little tilt and even negative wind shears above 950 hPa. Third, to examine whether or not the large-scale forcing would have any contribution to the cyclogenesis, a sensitivity simulation was conducted in which both the grid-scale latent heat release and the convective schemes were turned off *after the first 24-h integration* (experiment NLH), while keeping all the other model features identical to the control simulation (experiment CTL). In the absence of convective forcing (see Fig. 14), an 84-h integration produces a large-scale frontal trough, superposed with the perturbation associated with the vortex/trough to the south due to the anticyclonic influence of the subtropical high. The minimum pressure of 1015 hPa is almost the same as that left behind by the previous MCSs at 20/12-24 (cf. Figs. 6 and 14); it is about 14 hPa weaker than the control simulated (cf. Figs. 13b and 14). Meanwhile, the simulated maritime boundary layer ahead of the front is a little colder than that in experiment CTL.

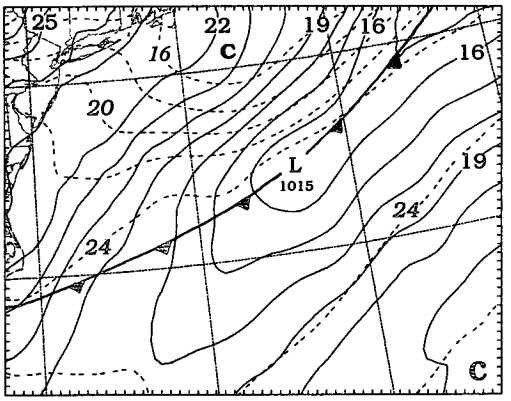

FIG. 14. As in Fig. 6 but for 84-h integration of experiment NLH (no latent heating).

These results reveal clearly that the large-scale baroclinic forcing makes small, if at all, contributions to the deepening of the oceanic cyclone, and the genesis occurs primarily as a consequence of the convective forcing associated with the oceanic storm.

At the end of the 90-h control integration, that is, at 23/06-90, the surface cyclone experienced a further deepening to 998 hPa (Fig. 15). It continues to deepen thereafter as it propagates rapidly northeastward. After another 6 h, however, the cyclone center is displaced outside of the fine-mesh domain; so the integration for the purpose of the present study is terminated at this hour. This time appears to mark the merging of the surface front with the cyclone, since the θ_e pattern (not shown) becomes more linear with its peak values distributed along the major pressure trough axis. This merging gives rise to the analysis of a new surface front along the pressure trough that is mostly generated by deep convection along the oceanic storm. Thus, the large-scale baroclinic forcing begins to have more significant influence on the evolution of the oceanic storm hereafter.

The importance of the convective forcing during the previous 42 h (i.e., from 21/12-48 to 23/06-90) can be further seen by inspecting the distribution and amount of the model-produced rainfall with respect to the track of the surface cyclone. Figure 16 shows that the model produces widespread precipitation over most of the ocean area within the subdomain, with considerable rainfall (>125 mm) occurring to the south and much less to the north of the cyclone's track. This pattern is consistent with the continued development of deep convection south of 35°N and the weak frontal cloud activity (cf. Figs. 3c–f and 16). Of special interest is that in spite of the continued convective development, little stratiform precipitation is generated along the path of the oceanic storm. The stratiform rainfall that occurred to the north of the track is relatively

averaged sense due to the collective effects of deep convection (i.e., upward motion) coupled with the cyclonic flow. In reality, air parcels embedded in (meso-γ-scale) convective updrafts or downdrafts tend to move more vertically than horizontally. Thus, this concept differs from that in a typical baroclinic system in which weak, stable ascent often occurs along frontal zones.

small (<15 mm) and associated with the lifting of high-θ_e air in the return flow along the "warm front." This result is in significant contrast to that which occurred within the continental MCSs, in which a substantial amount of stratiform precipitation (with a point maximum of 75 mm) is produced (e.g., see Fig. 13 in Zhang et al. 1988). This difference in the rainfall amount could be attributed to the different large-scale environments in which these two storms are embedded. Specifically, the continental MCSs are initiated in a near-saturated environment that was produced by the repeated formation of deep convection as the meso-α-scale short-wave trough and associated MCSs propagated from South Dakota toward Pennsylvania during a 3-day period (see BS81). By comparison, the oceanic storm develops in an environment under the long-period influence of the subtropical high so that the middle to upper tropospheres are extremely dry. The maintenance of the oceanic storm is primarily determined by the convective destabilization processes associated with the upward transfer of sensible and latent fluxes over the warm ocean, and their interactions with convectively generated circulations.

In summary, the convective forcing alone produces a total of 16-hPa deepening since its redevelopment 48 h earlier (see Fig. 5 and cf. Figs. 6 and 15). This spinup timescale is much shorter than that in tropical cyclogenesis (e.g., see Fig. 25 in Kurihara and Tuleya 1981). This difference appears to be attributable to the different environmental conditions under which oceanic cyclogenesis takes place. In the present case, the large-scale environment has a relatively stronger westerly mean flow, and perhaps more importantly a larger background vorticity (i.e., f).

4. Evolution of midlevel flows

As shown by BS81, ZF86, and ZF87, the development of the continental MCSs is always accompanied by a midlevel meso-α-scale short-wave trough and its

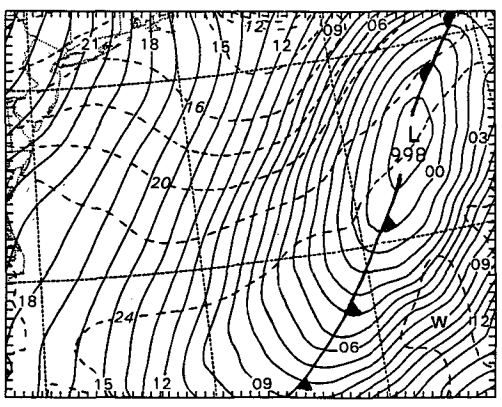

FIG. 15. As in Fig. 6 but from 90-h integration (23/06-90).

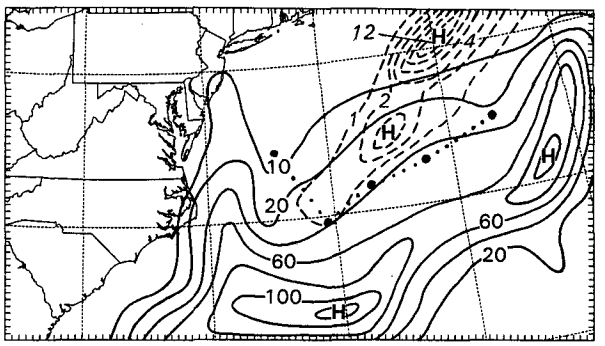

FIG. 16. The model-produced 42-h accumulated rainfall (mm) between 1200 UTC 21 and 0600 UTC 23 July 1977. Solid (dashed) lines are for convective (grid-scale) rainfall at intervals of 20 mm (2 mm) for the amounts larger than 20 mm (2 mm). Dotted line denotes the track of the surface cyclone center (see Fig. 1).

associated balanced vortex. This trough/vortex system also plays an important role in the organization of the oceanic storm, as will be discussed in the next section. In addition, a subtropical high to the south and a polar cold front from the north (see Fig. 2) appear to determine the movement of the cyclone/storm system. Thus, it is desirable to examine the structures and evolution of these larger-scale circulations in relation to the cyclogenesis over the ocean. For this purpose, Fig. 17 shows the evolution of the mesovortex, as represented by relative vorticity and wind vectors at 700 hPa, from 24-, 60-, and 84-h integrations, whereas Fig. 18 displays the corresponding large-scale circulations. These three periods are chosen since they represent roughly the dissipated stage of the continental MCSs, and the incipient and mature stages of the oceanic cyclone/storm system. The reader is referred to BS81, ZF86, and ZF87 for the larger-scale circulations at earlier times.

The midlevel flow at 20/12-24 exhibits a closed vortex circulation with concentrated cyclonic vorticity at the end of the continental MCC's life cycle (Fig. 17a). An examination of the mass field reveals that this vortex is more or less in gradient balance with a midlevel short-wave trough (cf. Figs. 17a and 18a). Similar scenarios also occurred at the early stages of tropical cyclogenesis during TEXMEX in which midlevel vortex circulations were collocated with the axes of easterly waves (see Emanuel et al. 1993). A comparison between Figs. 18a and 2a shows that the trough/vortex system has intensified appreciably as a result of the convective development over land. The low-level warm advection, though reduced considerably, still persists to the rear of the vortex/trough system. In contrast, the subtropical high has weakened slightly in intensity and shrunk in area coverage. Even so, the vortex/trough system is still embedded in the anticyclonic flow associated with the high. Thus, the vortex system tends to propagate southeastward into a tropical-like

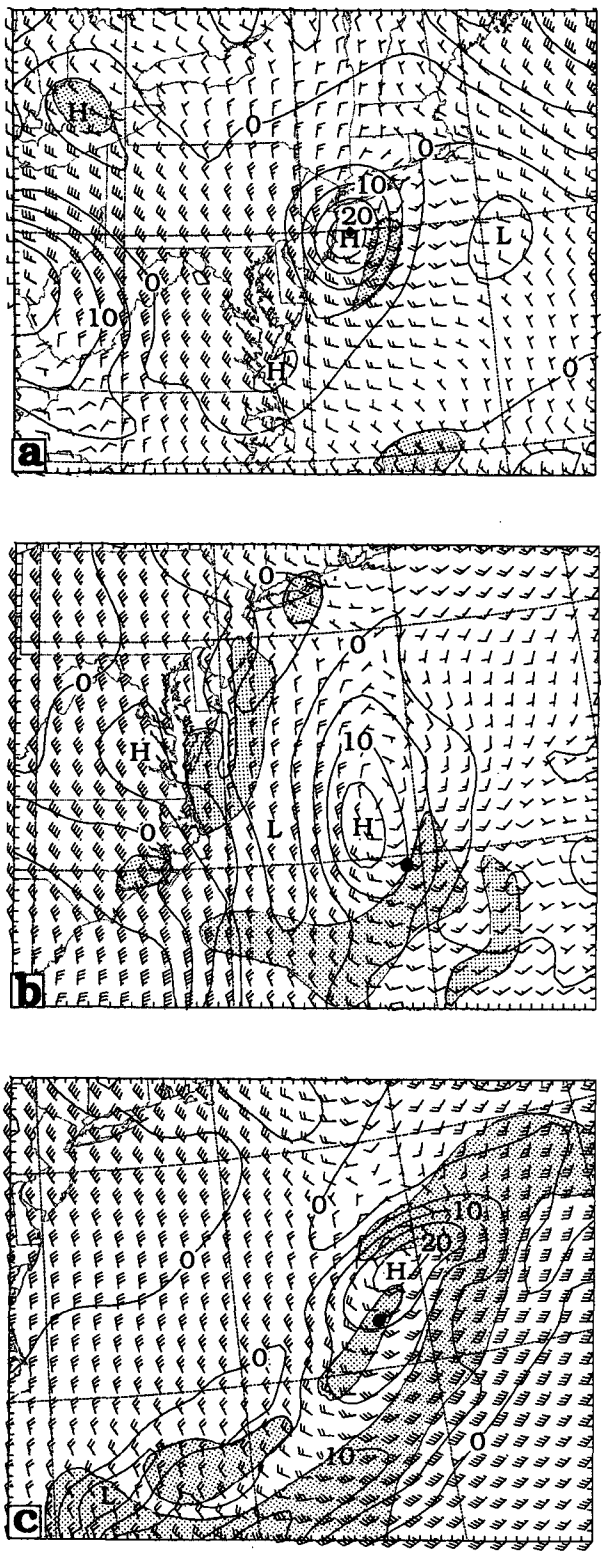

FIG. 17. Horizontal maps of simulated 700-hPa winds plotted at every other grid point and vertical relative vorticity at intervals of 5 $\times 10^{-5}$ s^{-1} at (a) 20/12-24, (b) 22/00-60, and (c) 23/00-84. A full wind barb is 5 m s^{-1}. Solid circle denotes the surface cyclone center. Shading shows the distribution of the oceanic storm.

environment, that is, with much weaker gradients (see Figs. 6–9). In the meantime, the developing baroclinic wave with strong thermal gradients is fast approaching from the northwest.

At 22/00-60, that is, 42 h after the dissipation of the continental MCC, the mesovortex is still well maintained in the absence of other convective forcing (Fig. 17b); but its intensity has weakened somewhat due partly to the application of numerical diffusion and partly to the influence of (weak) larger-scale deformational flow. These diffusive effects result in an area expansion of the vortex circulation (cf. Figs. 17a,b). Fritsch et al. (1994) have also noted an increase of the vortex scale after each life cycle of the MCS they analyzed. It is of interest to note that the surface cyclogenesis occurs at 150–180 km to the southeast of the vortex center (see Fig. 1 and cf. Figs. 9b and 17b), a feature that has been observed during TEXMEX (Emanuel et al. 1993). The tracks of the two systems tend to depart further hereafter (see Fig. 1). It is also of interest to note that as the vortex/trough system moves southeastward, surface pressure gradients to the southeast are intensifying with time, as mentioned before, whereas they are weakening right beneath the midlevel vortex (cf. Figs. 17b, 7b, 8b, and 9b). While dispersion of warm air away from the vortex columns could account for the continued weakening of the surface trough, we may consider the process given below as an alternative explanation for the phenomenon. Just imagine what would happen with surface isobars when a vertically coherent lower-pressure column is forced to move away from the eastwardly propagating baroclinic system to the north into the slowly evolving subtropical high to the southeast (see Figs. 2 and 18). This will cause an increase in the surface pressure gradient and thus the surface flow ahead, but a decrease in them in the wake. This scenario appears to reflect the important characteristics of the weak-gradient flows and the vertically coherent thermal structure of the vortex/trough system during its southeastward movement. The weak surface pressure gradients could clearly provide a favorable condition for the organization of cyclonic flow when cyclonic vorticity is locally generated or advected into the region; see appendix A of Part II for further discussion. This is because little pressure gradient force will be imposed on the parcels changing directions along their trajectories.

During the previous 36-h period, there have been some important changes in the large-scale circulations. Specifically, the area coverage of the subtropical high has decreased substantially as it drifts westward to the south of the approaching baroclinic wave (Fig. 18b). These evolutionary features of the subtropical high conform well to the NMC analysis (not shown). By comparison, the short-wave trough propagates southeastward to lower latitudes, but with little change in intensity. More significantly, the trough axis has shifted from its southwest–northeast orientation to south–

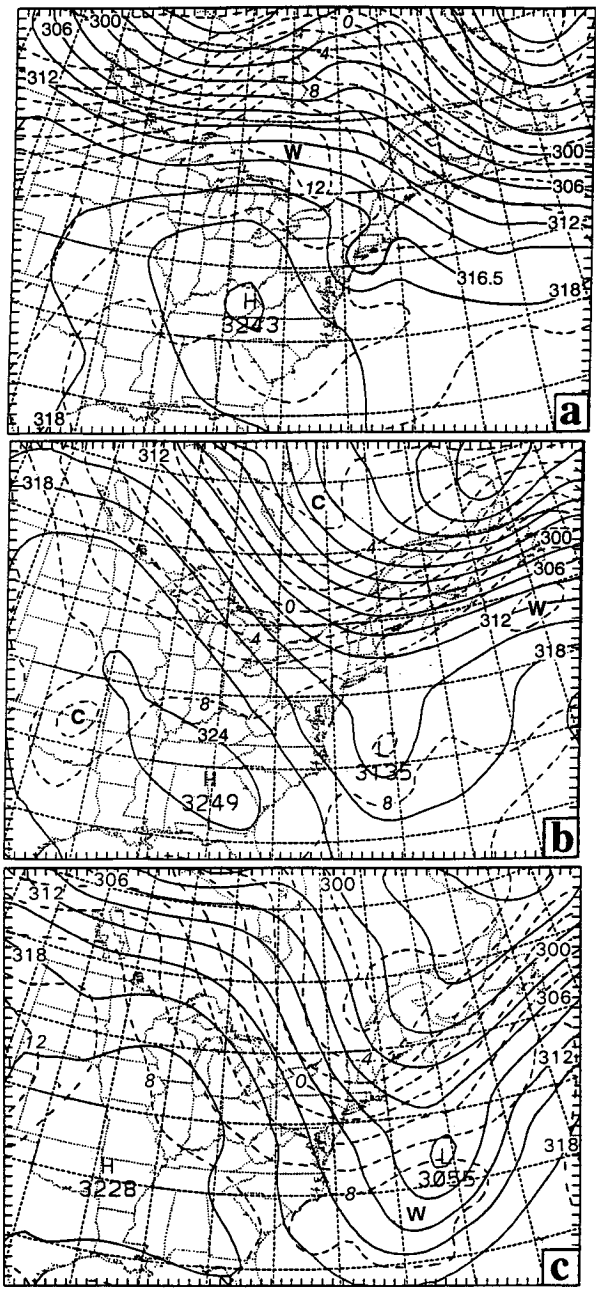

FIG. 18. As in Fig. 2a but from the simulations at (a) 20/12-24, (b) 22/00-60, and (c) 23/00-84.

north, so the vortex system looks like it is attached to the large-scale trough to the north instead of being superposed on the subtropical ridge at earlier times (cf. Figs. 2a and 18b). This shift appears to explain why the storm changes its direction of movement from southeastward to northeastward around 22/00-60 (see Fig. 1). It is evident that the mesovortex, after moving to the warm Gulf Stream water, is embedded in an environment with the thermal gradient much weaker than that which ever occurred before (cf. Figs. 2a and 18a,b). This indicates that the ensuing surface cyclogenesis takes place in a more barotropic environment with weak thermal advection or weak influence, if at all, from the baroclinic wave to the north, even at 850 hPa (not shown). This can be further seen from the propagation of a warm tongue (or thermal ridge) to the north of the vortex, that is advected through by the westerly flow from eastern Ontario at 20/12-24 to the south of Newfoundland at this hour, as indicated by the letter, "W," in Figs. 18a,b.

By 23/00-84, the short-wave trough has deepened 80 m during the previous 24-h period (see Fig. 18c). Associated with the mass deficit is the amplification of the midlevel mesovortex (as a result of the vortex stretching and advection, see Fig. 17c). Furthermore, the southwesterly wind speeds ahead of the trough axis have more than doubled, and the influence of the intense flow has spread over a much greater area in the southeastern quadrant due to the continued convective development. Of particular importance is that the vortex center is always located in the wake of the continental and oceanic storms (see Figs. 3–5 in ZF87 and Figs. 17a–c herein). This region appears to be a favorable location for the maintenance of a vortex, since the convective storms behave like an "obstacle" to its environmental flows such that the vortex could be protected from being rapidly sheared off. It should be pointed out that this convection–vortex juxtaposition differs from the warm-core vortex/MCSs case of July 1982 documented by Fritsch et al. (1994), in which deep convection repeatedly developed near the vortex center, rather than at the edge of vortex circulations. The vertical structure of the vortex circulations will be presented in Part II.

Although the large-scale trough, that is in a favorable phase with the thermal wave, has moved very close to that of the midlevel mesovortex, it has a separate circulation structure from that of the oceanic cyclone (Fig. 18c). Therefore, this points to the same conclusion that the oceanic cyclogenesis occurs in a near-barotropic environment with weak forcing, if at all, from the large-scale baroclinic system to the north up to this hour. On the other hand, the steering flow ahead of the large-scale trough axis tends to have more important influence on the subsequent movement of the cyclone/storm system.

5. Initiation and organization of the oceanic storm

In this section, we attempt to clarify how the oceanic storm is initiated near the North Carolina coast around 21/00-36 and then organized at 22/00-60 as the convectively generated perturbations move offshore (see Figs. 3, 7–9). To isolate the roles of the mesoscale perturbations in initiating and organizing the oceanic storm, we feel it more appropriate to examine mesoscale flow structures without the influence of diabatic

heating (after first 24-h integration), that is, through the analysis of experiment NLH. Without deep convection, the model atmospheric circulation will be dominated by the large-scale flows and mesoscale disturbances left behind by the dissipated MCC (e.g., cold outflows, surface pressure perturbations, and the vortex/trough) interacting with topography, land–ocean contrasts, and surface fluxes.

Figure 19 shows the distribution of sea level pressure, temperature, horizontal flow, and divergence at $\sigma = 0.873$ from 24-h NLH integration. At the end of the continental MCC's life cycle, we see a pool of cold air centered over New Jersey, which tilts downward toward the surface trough (Fig. 19a). Associated with the cold pool is an area of divergence, surrounded by a broad cyclonic flow with weak convergence. As will be shown in Part II, this broad cyclonic flow/cold pool is part of the mesovortex circulation. The convective line, "D," shown in Fig. 6, occurs just slightly behind the leading edge of the cold pool as a result of the lifting of high-θ_e air ahead. Over the land, the leading cold air has propagated rapidly into central North Carolina at the lee side of the Appalachians. This portion of cold outflow does not cause any development of new convection during the morning hours in spite of a favorable convergence zone behind the leading edge (Fig. 19b). This is consistent with the analyses of H78 (see Fig. 4) and BS81 (see their Fig. 9), since this region is conditionally stable (Fig. 19a) and since the major dynamic forcing (i.e., organized mass convergence) is still associated with the midlevel short-wave trough/vortex (cf. Figs. 18a and 19b). It should be noted, though, that the divergence/convergence patterns in the vicinity of the Appalachians have been influenced by the topography, such as the divergence zone over West Virginia and part of the convergence downstream; but the orographic effects are relatively small offshore.

At 21/00-36, the main cold pool and the associated divergence have moved offshore[9] (see Fig. 20). In contrast, the portion of cold downdraft air mass over the land diminishes rapidly as the daytime PBL develops, and after a diurnal cycle a warm pocket appears in the lee of the Appalachians. Obviously, the continental warm air now begins to overrun the maritime cold pool in the presence of the meso-α-scale cyclonic flow, namely, potential temperature θ tilts upward along the current. This results in favorable convergence and upward lifting over the coastal region. Since this region is also distributed with conditional instability, the convective development should occur as expected (cf. Figs. 20b and 7b). On the other hand, the favorable

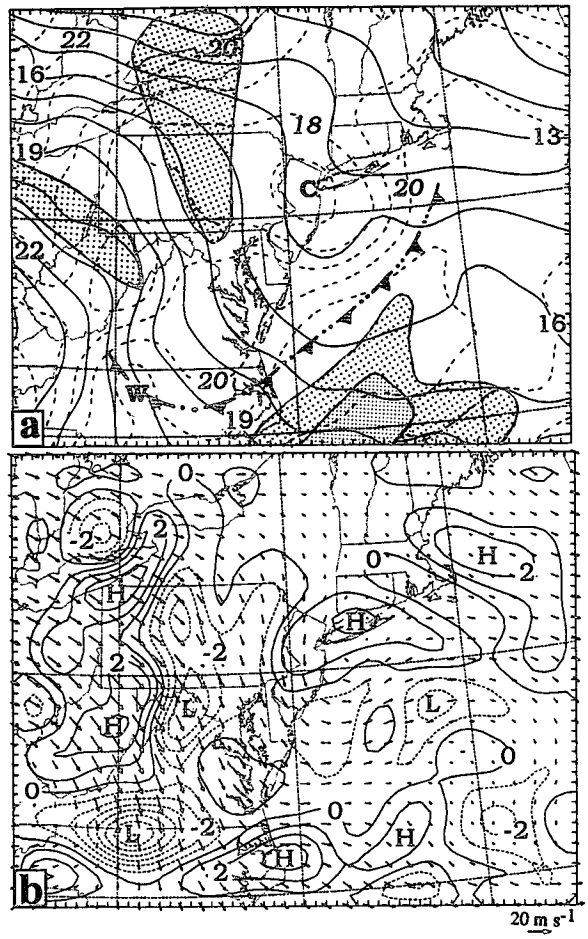

FIG. 19. (a) Sea level pressure (solid, every 1 hPa), superposed with temperature (dashed, every 1°C) at $\sigma = 0.873$ (i.e., about 85 hPa above the surface) from 24-h integration of experiment NLH. Letters "L," "W," and "C" denote the centers of low pressure, warm air, and cold air, respectively. Frontal symbols alternated with double dots indicate cold outflow boundaries. Coarse (dense) shading shows the distribution of $\Delta\theta_e$ between $\sigma = 0.647$ and 0.929 (roughly with $\Delta p = 265$ hPa), i.e., less than -20 (-25) K. (b) Horizontal divergence (positive/solid, negative/dashed) at $\sigma = 0.873$ at intervals of 10^{-5} s^{-1}, superposed with wind vectors.

convergence at the southern periphery of the cold pool/vortex persists during the previous 12 h (see Figs. 19b and 20b). While deep convection fails to develop over the convergence zone, the continuous upward lifting of high-θ_e air in the maritime boundary layer may help condition the prestorm environment for the subsequent eastward expansion of the new convection. It follows that the new convective system at the North Carolina coast, shown in Fig. 3b, is initiated at the southern periphery of the mesovortex as a consequence of the cyclonic circulations interacting with the land–ocean thermal contrasts during the afternoon hours. When the surface diurnal heating cycle was turned off after the 24-h integration, the model was unable to reproduce

[9] Note that because the cold pool tends to subside with time, all fields are presented at $\sigma = 0.873$ (about 85 hPa above the surface) for the 24-h integration and at $\sigma = 0.929$ (about 60 hPa above the surface) for the 36-h integration.

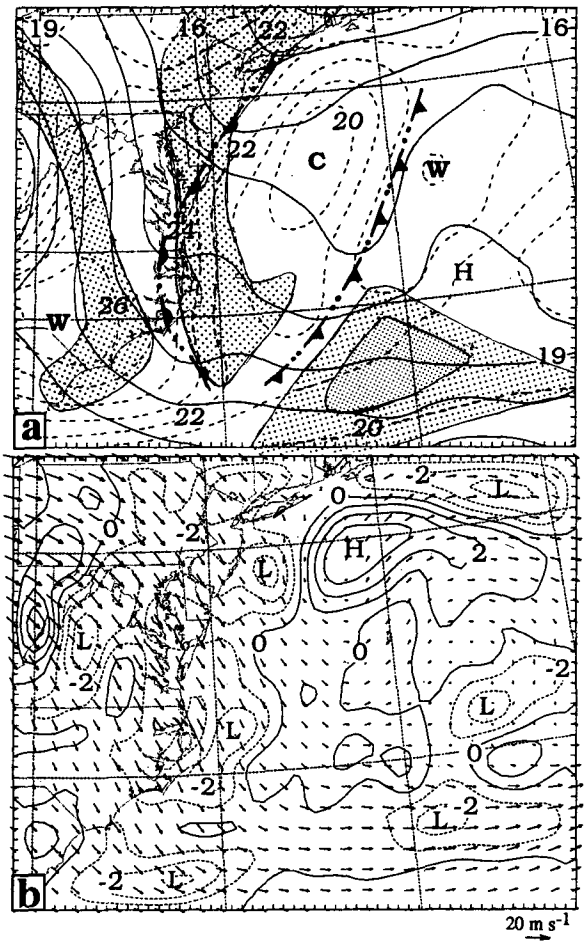

FIG. 20. As in Fig. 19 but at $\sigma = 0.929$ (about 60 hPa above the surface) from 36-h integration of experiment NLH.

deep convection along the coast at 21/00-36 (not shown).

The organization of the new convection into the oceanic storm certainly depend on whether or not there are (i) a continued supply of convective available potential energy (CAPE) and (ii) a mesoscale forcing mechanism to persistently focus the CAPE such that the centralized convective heating, interacting with the surface fluxes over the warm Gulf Stream water, can result in a highly organized MCS. As mentioned previously, surface pressure gradients and winds ahead of the trough axis in experiment CTL intensify rapidly as the mesovortex moves southeastward under the influence of the subtropical high (cf. Figs. 6–9 and 17–18). Similar scenarios occur more or less in experiment NLH (cf. Figs. 19a, 20a, and 21a), except that the model is unable to reproduce a surface mesolow and very weak pressure gradients beneath the vortex (due to the presence of vertically less coherent thermal structures). Nonetheless, a favorable and persistent mesoscale forcing is evident ahead of the trough axis, even in the absence of deep convection (see Figs. 19–21). The significance of the trough/vortex in organizing the oceanic storm can be further seen by comparing Figs. 21a,b and 9b, which show that the southwest–northeast elongated boundary layer convergence and conditionally unstable zone in experiment NLH resembles so well the distribution of the simulated convective band at 22/00-60.

The next issue is the source of high-θ_e air and its transport into the region of release. As shown in Fig. 21, the low-level jetlike flow, resulting from the increased pressure gradients, generates a warm tongue in the southwesterly flow due partly to the upward sensible heat flux from the warm water, and partly to the warm advection from the heated PBL over the land (cf. Figs. 20a and 21a) and from the lower latitudes where ample high-θ_e air is available. Note that the large-scale warm advection decreases rapidly with height and it almost vanishes at 700 hPa (see Fig. 18b). Since the ambient winds exhibit negative vertical shear above 950 hPa (see Fig. 4 in Part II), this thermal structure

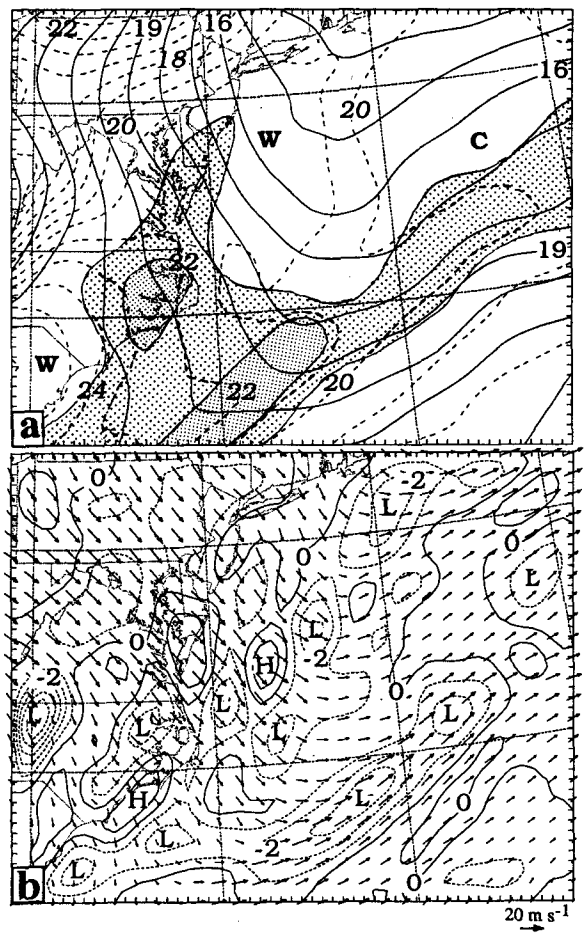

FIG. 21. As in Fig. 19 but at $\sigma = 0.929$ (about 60 hPa above the surface) from 60-h integration of experiment NLH.

due to differential thermal advection and surface fluxes tends to destabilize atmospheric columns along the way. This is evidenced from Fig. 21a, which displays an extensive area of conditional instability in the southwesterly flow. This trend persists at least for the subsequent 30 h (not shown). Therefore, we may state that the persistent forcing from the inertially stable trough/vortex system, the low-level warm advection over the mid-Atlantic states and the steady CAPE supply (through upward surface fluxes) from the tropic ocean account for the continued development and organization of the oceanic storm (see Figs. 6–9), and determine the predictability of the storm/cyclone system beyond 2.5 days. It is evident that when deep convective effects are included, the CAPE supply from the tropic ocean will be more pronounced. This will be shown in the context of heat budgets in Part II. It should be noted, though, that the weak surface drag is also an important parameter in assisting the convective development through generation of stronger surface cyclonic flows and enhanced surface fluxes. The above statement is confirmed by a sensitivity simulation in which the ocean surface characteristics are replaced by typical land conditions. In this simulation, to be presented in a forthcoming journal article, the model reproduces reasonably well the continued convective development but fails to generate the surface cyclone.

6. Summary and conclusions

In this paper, we have demonstrated the mesoscale predictability of oceanic cyclogenesis from an MCS out to 90 h using an improved version of the PSU–NCAR mesoscale model with a fine-mesh grid size of 25 km. This work is an extension of the previously documented 18-h simulation of the MCSs, that were responsible for the Johnstown flash flood of July 1977, by ZF86, ZF87, Zhang et al. (1988), and Zhang (1989). The improved version of the model uses (i) the Kain–Fritsch cumulus scheme instead of the Fritsch–Chappell scheme, and (ii) a modified version of the Grand infrared radiation scheme. It has been shown in our earlier studies that the model reproduces very well the development of a squall line and an MCC, surface mesolows, mesohighs and outflow boundaries, a midlevel short-wave trough and a mesovortex, and the magnitude and distribution of precipitation, as verified against the mesoanalyses of H78 and BS81. In the present study, comparisons of the simulation with the documentation of BS81 and satellite observations show further the capabilities of the model in reproducing much of the meso-β-scale structure and evolution of the long-lived MCSs out to 90 h. These include (i) the dissipation of the MCC and the weakening of the surface mesolow to a mesotrough as they move away from the state of Pennsylvania; (ii) the timing and location of the initiation of a new MCS at 36-h integration and the genesis of a surface mesolow at the south periphery of the previous trough/vortex system over the warm Gulf Stream water after 60 h into the integration; (iii) the subsequent track and deepening of the surface cyclone; (iv) the orientation and area coverage of the oceanic storm with respect to the surface cyclone; (v) the development of tropical-storm-like surface winds; (vi) the maintenance of the mesovortex/trough system; (vii) the westward retreat and weakening of a subtropical high; and (viii) the propagation of a large-scale cold front and a midlevel baroclinic wave in relation to the oceanic storm/cyclone system.

It is found that the new MCS is initiated at the southern periphery of the mesovortex at 21/00-36, after the vortex/cold-pool moved offshore and interacted with the land–ocean thermal boundaries during the afternoon hours. Meanwhile, as the surface trough advances toward the warm Gulf Stream water at lower latitudes under the influence of the subtropical high, it weakens but the pressure gradients ahead of the trough axis and the associated southwesterly flow intensify with time. The intensifying flow helps enhance mesoscale convergence in the PBL and organize the deep convection into the oceanic storm at the southern periphery of the previously dissipated MCC. Furthermore, the intensifying flow tends to (i) "pump" up sensible and latent heat fluxes from the warm ocean surface; and (ii) transport the tropical higher-θ_e air in a cyclonic-slantwise fashion into the region having lower-θ_e aloft, thereby producing further conditional instability, enhanced deep convection and increased cyclonic deepening. These processes, enhanced by mesoscale ascent, appear to be responsible for the wrapping-around of high-θ_e air and the development of "comma-shaped" deep convection during the mature stage of the storm; see Part II for more quantitative aspects of the wrapping-around processes. It is found that the mesovortex plays an important part in assisting the initiation and organization of the oceanic storm and its associated flow structures.

The roles of deep convection versus large-scale forcing in the oceanic cyclogenesis have been investigated. It is shown that the oceanic cyclone/storm system develops within a prefrontal, near-barotropic environment. The subtropical high helps steer the propagation of the vortex/trough system prior to 22/00-60, whereas the large-scale baroclinic wave to the north plays a role in determining the movement of the cyclone/storm system and its intensity near the end of the 90-h integration. In the absence of deep convection, an 84-h sensitivity simulation produces only a surface trough with its minimum pressure being nearly the same as that left behind by the previous MCSs at 20/12-24. It is found that the cyclogenesis begins between 21/12-48 and 22/00-60 at 150–180 km to the southeast of the vortex/trough, with the surface mesolow hugged by the oceanic storm. The oceanic cyclone, once initiated, spins up rapidly and overpowers the low-level portion of the vortex/trough circulation; it deepens 14 hPa in 24 h.

The genesis is shown to be driven entirely by the parameterized deep convection along the oceanic storm with little contribution from grid-scale precipitation. Therefore, we may conclude that the oceanic cyclogenesis in the present case is *induced by the continental MCS/vortex system at its southern periphery,* after it moved into the warm Gulf Stream water, and then it is *driven by deep convection associated with the oceanic storm* in the southwest-to-southerly flow of tropical high-θ_e air. In Part II of this series of papers, we will examine how various dynamic and thermodynamic processes are responsible for the transformation of the continental MCS/vortex to the oceanic cyclone/storm system.

Acknowledgments. We are very grateful to Mike Fritsch for his continuing interest and support during the course of this project. We thank Louis Garand of Recherche en Prévision Numérique of the Atmospheric Environment Service for guiding our use of his radiation–cloud interaction scheme. Thanks also go to Lance Bosart and Fred Sanders for providing the satellite imagery and their original surface maps for the present study. The computations were performed on the CRAY Y-MP (Shavano) at the National Center for Atmospheric Research (NCAR) under Grant ATM-92-22017. NCAR is sponsored by the National Science Foundation. This research was supported by the Natural Sciences and Engineering Research Council of Canada.

REFERENCES

Anthes, R. A., 1982: *Tropical Cyclones: Their Evolution, Structure and Effects.* American Meteorological Society, 208 pp.

——, and D. P. Baumhefner, 1984: A diagram depicting forecast skill and predictability. *Bull. Amer. Meteor. Soc.,* **65,** 701–703.

——, E.-Y. Hsie, and Y.-H. Kuo, 1987: Description of the Penn State/NCAR mesoscale model version 4 (MM4). NCAR Tech. Note NCAR/TN-282, 66 pp.

Augustine, J. A., and K. W. Howard, 1988: Mesoscale convective complexes over the United States during 1985. *Mon. Wea. Rev.,* **116,** 685–701.

——, and ——, 1991: Mesoscale convective complexes over the United States during 1986 and 1987. *Mon. Wea. Rev.,* **119,** 1575–1589.

Bartels, D. L., and R. A. Maddox, 1991: Midlevel cyclonic vortices generated by mesoscale convective systems. *Mon. Wea. Rev.,* **119,** 104–118.

Benoit, R., J. Cote, and J. Mailhot, 1989: Inclusion of a TKE boundary-layer parameterization in the Canadian regional finite-element model. *Mon. Wea. Rev.,* **117,** 1726–1750.

Black, P. G., and G. J. Holland, 1995: The boundary layer of Tropical Cyclone Kerry (1979). *Mon. Wea. Rev.,* **123,** 2007–2028.

Bosart, L. R., and F. Sanders, 1981: The Johnstown flood of July 1977: A long-lived convective storm. *J. Atmos. Sci.,* **38,** 1616–1642.

Burpee, R. W., 1986: Mesoscale structure of hurricanes. *Mesoscale Meteorology and Forecasting,* P. S. Ray, Ed., American Meteorological Society, 311–330.

Cotton, W. R., R. L. George, P. J. Wetzel, and R. L. McAnelly, 1983: A long-lived mesoscale convective complex. Part I: The mountain-generated component. *Mon. Wea. Rev.,* **111,** 1893–1918.

——, M. S. Lin, R. L. McAnelly, and C. J. Tremback, 1989: A composite model of mesoscale convective complexes. *Mon. Wea. Rev.,* **117,** 765–783.

Davis, C. A., and M. L. Weisman, 1994: Balanced dynamics of mesoscale vorticies produced in simulated convective systems. *J. Atmos. Sci.,* **51,** 2005–2030.

Dudhia, J., 1989: Numerical study of convection observed during the winter monsoon experiment using a mesoscale two-dimensional model. *J. Atmos. Sci.,* **46,** 3077–3107.

Emanuel, K. A., 1986: An air–sea interaction theory for tropical cyclones. Part I: Steady state maintenance. *J. Atmos. Sci.,* **43,** 585–604.

——, N. Renno, L. R. Schade, M. Bister, M. Morgan, D. Raymond, and R. Rotunno, 1993: Tropical cyclogenesis over the eastern North Pacific: Some results of TEXMEX. Preprints, *20th Conf. on Hurricanes and Tropical Meteorology,* San Antonio, TX, Amer. Meteor. Soc., 110–113.

Fritsch, J. M., and C. F. Chappell, 1980: Numerical prediction of convectively driven mesoscale pressure systems. Part I: Convective parameterization. *J. Atmos. Sci.,* **37,** 1722–1733.

——, and R. A. Maddox, 1981: Convectively driven mesoscale weather systems aloft. Part I: Observations. *J. Appl. Meteor.,* **20,** 9–19.

——, and J. M. Brown, 1982: On the generation of convectively driven mesohighs aloft. *Mon. Wea. Rev.,* **110,** 1554–1563.

——, R. J. Kane, and C. R. Chelius, 1986: The contribution of mesoscale convective weather systems to the warm-season precipitation in the United States. *J. Climate Appl. Meteor.,* **25,** 1333–1345.

——, J. D. Murphy, and J. S. Kain, 1994: Warm-core vortex amplification over land. *J. Atmos. Sci.,* **51,** 1780–1807.

Garand, L., 1983: Some improvements and complements to the infrared emissivity algorithm including a parameterization of the absorption in the continuum region. *J. Atmos. Sci.,* **40,** 230–244.

Gray, W. M., 1979: Hurricanes: Their formation, structure, and likely role in the tropical cyclones. *Meteorology over the Tropical Oceans,* D. B. Shaw, Ed., Royal Meteorological Society, 155–218.

Hoxit, L. R., R. A. Maddox, C. F. Chappell, F. L. Zuckerberg, H. M. Mogil, I. Jones, D. R. Greene, R. E. Saffle, and R. A. Scofield, 1978: Meteorological analysis of the Johnstown, Pennsylvania flash flood, 19–20 July 1977. NOAA Tech. Rep. ERL 401-APCL43, 71 pp.

Hsie, E.-Y., R. A. Anthes, and D. Keyser, 1984: Numerical simulation of frontogenesis in a moist atmosphere. *J. Atmos. Sci.,* **41,** 2581–2594.

Kain, J. S., and J. M. Fritsch, 1990: A one-dimensional entraining/detraining plume model and its application in convective parameterization. *J. Atmos. Sci.,* **47,** 2784–2802.

——, and ——, 1993: Convective parameterization for mesoscale models: The Kain–Fritsch scheme. *The Representation of Cumulus Convection in Numerical Models, Meteor. Monogr.,* No. 46, Amer. Meteor. Soc., 165–170.

Krishnamurti, T. N., K. S. Yap, and D. K. Oosterhof, 1991: Sensitivity of tropical storm forecast to radiative destabilization. *Mon. Wea. Rev.,* **119,** 2176–2205.

Kurihara, Y., and R. E. Tuleya, 1981: A numerical simulation study on the genesis of a tropical storm. *Mon. Wea. Rev.,* **109,** 1629–1653.

Laing, A. G., and J. M. Fritsch, 1993: Mesoscale convective complexes over the Indian monsoon region. *J. Climate,* **6,** 911–919.

Maddox, R. A., 1980: Mesoscale convective complexes. *Bull. Amer. Meteor. Soc.,* **61,** 1374–1387.

——, 1983: Large-scale meteorological conditions associated with midlatitude mesoscale convective complexes. *Mon. Wea. Rev.,* **111,** 1495–1493.

——, D. M. Rodgers, and K. W. Howard, 1982: Mesoscale convective complexes over the United States during 1981—Annual summary. *Mon. Wea. Rev.,* **110,** 1501–1514.

Mapes, B. E., and R. A. Houze Jr., 1995: Diabatic divergence profiles in western Pacific mesoscale convective systems. *J. Atmos. Sci.,* **52,** 1807–1828.

McAnelly, R. L., and W. R. Cotton, 1989: The precipitation life cycle of mesoscale convective complexes over the central United States. *Mon. Wea. Rev.,* **117,** 784–808.

Menard, R. D., and J. M. Fritsch, 1989: A mesoscale convective complex-generated inertially stable warm core vortex. *Mon. Wea. Rev.,* **117,** 1237–1261.

Miller, D., and J. M. Fritsch, 1991: Mesoscale convective complexes in the western Pacific region. *Mon. Wea. Rev.,* **119,** 2978–2992.

Molinari, J., and M. Dudek, 1992: Parameterization of convective precipitation in mesoscale numerical models. A critical review. *Mon. Wea. Rev.,* **120,** 326–344.

Parsons, D., W. Dabberdt, H. Cole, T. Hock, C. Martin, A.-L. Barrett, E. Miller, M. Spowart, M. Howard, W. Ecklund, D. Carter, K. Gage, and J. Wilson, 1994: The integrated sounding system: Description and preliminary observations from TOGA COARE. *Bull. Amer. Meteor. Soc.,* **75,** 553–567.

Perkey, D. J., and C. W. Kreitzberg, 1976: A time-dependent lateral boundary scheme for limited-area primitive equation models. *Mon. Wea. Rev.,* **104,** 744–755.

Raymond, D. J., 1992: Nonlinear balance and potential-vorticity thinking at large Rossby number. *Quart. J. Roy. Meteor. Soc.,* **118,** 987–1105.

Rodgers, D. M., K. W. Howard, and E. C. Johnston, 1983: Mesoscale convective complexes over the United States during 1982—Annual summary. *Mon. Wea. Rev.,* **111,** 2363–2369.

——, M. J. Magnano, and J. H. Arns, 1985: Mesoscale convective complexes over the United States during 1983—Annual summary. *Mon. Wea. Rev.,* **113,** 888–901.

Rothman, L. S., and Coauthors, 1987: The HITRAN database: 1986 edition. *Appl. Optics,* **26,** 4058–4097.

Rotunno, R., and K. A. Emanuel, 1987: An air–sea interaction theory for tropical cyclones. Part II: Evolutionary study using a nonhydrostatic axisymmetric numerical model. *J. Atmos. Sci.,* **44,** 542–561.

Ryan, B. F., G. M. Barnes, and E. J. Zipser, 1992: A wide rainband in a developing tropical cyclone. *Mon. Wea. Rev.,* **120,** 431–447.

Schubert, W. H., and J. J. Hack, 1982: Inertial stability and tropical cyclone development. *J. Atmos. Sci.,* **39,** 1687–1697.

Stull, R. B., 1985: Predictability and scales of motion. *Bull. Amer. Meteor. Soc.,* **66,** 432–436.

Velasco, I., and J. F. Fritsch, 1987: Mesoscale convective complexes in the Americas. *J. Geophys. Res.,* **92,** 9591–9613.

Wallace, J. M., 1975: Diurnal variations in precipitation and thunderstorm frequency over the conterminous United States. *Mon. Wea. Rev.,* **103,** 406–419.

Webster, P. J., and R. Lukas, 1992: TOGA COARE: The coupled ocean–atmosphere response experiment. *Bull. Amer. Meteor. Soc.,* **73,** 1377–1416.

Wetzel, P. J., W. R. Cotton, and R. L. McAnelly, 1983: A long-lived mesoscale convective complex. Part II: Evolution and structure of the mature complex. *Mon. Wea. Rev.,* **111,** 1919–1937.

Zehr, R. M., 1992: Tropical cyclogenesis in the western North Pacific. NOAA Tech. Rep. NESDIS 61, 181 pp.

Zhang, D.-L., 1989: The effect of parameterized ice microphysics on the simulation of vortex circulation with a mesoscale hydrostatic model. *Tellus,* **41A,** 132–147.

——, and R. A. Anthes, 1982: A high-resolution model of the planetary boundary layer—Sensitivity tests and comparison with SESAME-79 data. *J. Appl. Meteor.,* **21,** 1594–1609.

——, and J. M. Fritsch, 1986: Numerical simulation of the meso-β-scale structure and evolution of the 1977 Johnstown flood. Part I: Model description and verification. *J. Atmos. Sci.,* **43,** 1913–1943.

——, and ——, 1987: Numerical simulation of the meso-β-scale structure and evolution of the 1977 Johnstown flood. Part II: Inertially stable warm-core vortex and the mesoscale convective complex. *J. Atmos. Sci.,* **44,** 2593–2612.

——, and ——, 1988a: A numerical investigation of a convectively generated, inertially stable, extratropical warm-core mesovortex over land. Part I: Structure and evolution. *Mon. Wea. Rev.,* **116,** 2660–2687.

——, and ——, 1988b: Numerical sensitivity experiments of varying model physics on the structure, evolution and dynamic of two mesoscale convective systems. *J. Atmos. Sci.,* **45,** 261–293.

——, and N. Bao, 1996: Oceanic cyclogenesis as induced by a mesoscale convective system moving offshore. Part II: Model diagnosis and budgets. *Mon. Wea. Rev.,* in press.

——, H.-R. Chang, N. L. Seaman, T. T. Warner, and J. M. Fritsch, 1986: A two-way interactive nesting procedure with variable terrain resolution. *Mon. Wea. Rev.,* **114,** 1330–1339.

——, E.-Y. Hsie, and M. W. Moncrieff, 1988: A comparison of explicit and implicit prediction of convective and stratiform precipitating weather systems with a meso-β-scale numerical model. *Quart. J. Roy. Meteor. Soc.,* **114,** 31–60.

——, J. S. Kain, J. M. Fritsch, and K. Gao, 1994: Comments on "Parameterization of convective precipitation in mesoscale numerical models. A critical review." *Mon. Wea. Rev.,* **122,** 2222–2231.